Fabrication and characterization of cobalt- and copper-doped mesoporous borate bioactive glasses for potential applications in tissue engineering

Ceramics International 49 (2023) 38773–38788

Contents lists available at ScienceDirect

Ceramics International

journal homepage: www.elsevier.com/locate/ceramint

Fabrication and characterization of cobalt- and copper-doped mesoporous borate bioactive glasses for potential applications in tissue engineering

Zoleikha Azari [a,1], Farzad Kermani [b,1], Sahar Mollazadeh [c], Fatemeh Alipour [a], Alireza Sadeghi-Avalshahr [a,d], Marziyeh Ranjbar-Mohammadi [e], Bahman Jalali Kondori [a], Zahra Mollaei [c], Seyede Atefe Hosseini [f], Simin Nazarnezhad [b], Kai Zheng [g], Francesco Baino [h,*], Saeid Kargozar [b,**]

[a] Department of Anatomy and Cell Biology, School of Medicine, Mashhad University of Medical Sciences, Mashhad, 917794-8564, Iran
[b] Tissue Engineering Research Group (TERG), Department of Anatomy and Cell Biology, School of Medicine, Mashhad University of Medical Sciences, Mashhad, 917794-8564, Iran
[c] Department of Materials Engineering, Faculty of Engineering, Ferdowsi University of Mashhad (FUM), Azadi Sq., Mashhad, 917794-8564, Iran
[d] Department of Materials Research, Iranian Academic Center for Education, Culture and Research (ACECR), Khorasan Razavi Branch, Mashhad, Iran
[e] Department of Textile Engineering, University of Bonab, Bonab, 5551395133, Iran
[f] Department of Medical Biotechnology and Nanotechnology, Faculty of Medicine, Mashhad University of Medical Sciences, Mashhad, Iran
[g] Jiangsu Province Engineering Research Center of Stomatological Translational Medicine & Jiangsu Key Laboratory of Oral Diseases, Nanjing Medical University, Nanjing, 210029, China
[h] Institute of Materials Physics and Engineering, Applied Science and Technology Department, Politecnico di Torino, Corso Duca degli Abruzzi 24, 10129, Torino, Italy

ARTICLE INFO

Handling Editor: Dr P. Vincenzini

Keywords:
Mesoporous bioactive glass (MBGs)
Borate glasses
Data science
Biocompatibility
Tissues engineering

ABSTRACT

Developing novel compositions of bioactive glasses (BGs) is key for accelerating tissue repair and regeneration. In this work, we developed a series of cobalt (Co)- and copper (Cu)-doped mesoporous bioactive glasses (MBGs) based on borate 13-93B3 composition using nitrate precursors. We took benefit from data science algorithms to predict and assess the physico-chemical and biological properties of the samples. The results showed that the presence of the dopants (Co and Cu) in the MBGs could change the glass transition temperature (T_g) (from 773 to 539 °C), the zeta potential (from -12 to -43 mV), and surface area (from 54 to 194 m^2/g). However, the presence of 2.5 mol% of dopants in the composition led to just a slight decrease in their bioactivity. *In vitro* biocompatibility assays confirmed that all the glass samples were biocompatible. Furthermore, the doped MBGs exhibited potent antibacterial activity against both Gram-positive and Gram-negative bacteria. In addition, these glasses could induce the mobility of human umbilical vein endothelial cells (HUVECs) and enhance new blood vessel formation *in ovo*. According to the obtained data, it can be stated that this type of doped borate MBGs held great promise in tissue engineering applications.

1. Introduction

Researchers working in different fields have extensively utilized novel technologies for scientific data management in order to optimize procedures and processes [1,2]. In this regard, the demand for data processing has naturally increased in the field of materials science and engineering [3,4]. Over the past few years, scientists in the area of glass science have increasingly used data science skills to provide a deeper insight into the relationship between materials compositions and their properties [5,6]. On this matter, artificial intelligence (AI) and coding are among the most useful technologies applied for the prediction of scientific events [7]. For example, a new parameter has been introduced to the field of glass science using data science and molecular dynamics simulations, i.e., the correlation between entropy (a calculable thermodynamic parameter) and glass properties [8,9].

It is widely acknowledged that bioactive glasses (BGs) are among the

* Corresponding author.
** Corresponding author.
E-mail addresses: francesco.baino@polito.it (F. Baino), kargozarsaeid@gmail.com (S. Kargozar).
[1] These authors contributed equally to the work.

https://doi.org/10.1016/j.ceramint.2023.09.214
Received 12 May 2023; Received in revised form 7 September 2023; Accepted 19 September 2023
Available online 19 September 2023

Table 1
The nominal compositions of the various 13-93B3-based MBGs (mol%) produced in this work.

Sample	B_2O_3	CaO	CoO	CuO	MgO	K_2O	Na_2O	P_2O_5
B0	54.6	22.1	0	0	7.6	7.9	6.1	1.7
Co0.5	54.6	21.6	0.5	0	7.6	7.9	6.1	1.7
Co1	54.6	21.1	1	0	7.6	7.9	6.1	1.7
Co2.5	54.6	19.6	2.5	0	7.6	7.9	6.1	1.7
Cu0.5	54.6	21.6	0	0.5	7.6	7.9	6.1	1.7
Cu1	54.6	21.1	0	1	7.6	7.9	6.1	1.7
Cu2.5	54.6	19.6	0	2.5	7.6	7.9	6.1	1.7
Co/Cu 0.5	54.6	21.6	0.25	0.25	7.6	7.9	6.1	1.7
Co/Cu 1	54.6	21.1	0.5	0.5	7.6	7.9	6.1	1.7
Co/Cu 2.5	54.6	19.6	1.25	1.25	7.6	7.9	6.1	1.7

Table 2
A collection of data related to the MBGs analyses, including DTA, zeta potential, and BET/BJH. All data changes compared to the control group (B0) are significant ($p < 0.05$).

Analysis	DTA	Zeta potential	BET	BJH
Sample	**T_g (°C)**	**Zeta potential (mV)**	**S_{BET} (m^2/g)**	**Average pore diameter (nm)**
B0	773 ± 6	-(12 ± 4)	54 ± 2	23 ± 4
Co0.5	694 ± 9	-(26 ± 6)	75 ± 8	19 ± 2
Co1	640 ± 7	-(32 ± 3)	106 ± 4	13 ± 1
Co2.5	596 ± 13	-(36 ± 2)	126 ± 6	8 ± 2
Cu0.5	700 ± 5	-(19 ± 7)	60 ± 7	21 ± 3
Cu1	695 ± 9	-(21 ± 4)	66 ± 9	19 ± 1
Cu2.5	684 ± 4	-(20 ± 4)	76 ± 8	16 ± 2
Co/Cu 0.5	681 ± 8	-(27 ± 2)	79 ± 5	18 ± 3
Co/Cu 1	632 ± 9	-(34 ± 4)	123 ± 6	9 ± 1
Co/Cu 2.5	539 ± 6	-(43 ± 4)	194 ± 7	5 ± 2

most important members of the glass family for biomedical applications [10,11]. BGs have been previously proven to promote the repair and regeneration of both hard and soft tissues. As a first-generation BG product, silica-based 45S5 Bioglass® was developed for use in treating hard tissues (e.g., bone); then, the next generation of borate-based BGs was developed for potential use in soft tissue engineering (e.g., skin), too, in the early 2000s [12-14]. As compared with silicate glasses, lower temperatures are required for the heat treatment of borate-based BGs [15]. This is primarily stemmed from the fact that the glass transition temperature (T_g) and melting temperature (T_m) of pure B_2O_3 are much lower than the corresponding temperatures for SiO_2 (T_g of 260 versus 1100 °C, and T_m of 450 versus 1728 °C) [15]. Due to the poor chemical durability and high water affinity of pure B_2O_3, borate glasses are typically synthesized in complex compositions, such as 13-93B3 borate glass (e.g., B_2O_3–CaO–Na_2O–MgO–P_2O_5 system) [16]. Furthermore, due to the lower network connectivity (NC) of bioactive borate glasses (BBGs), the process of BBGs gelation is relatively complicated resulting in difficulties in their synthesis via the sol-gel method [16]. New studies have shown the possibility of synthesizing BBGs through using affordable and safe nitrate precursors instead of costly methoxy precursors by a modified sol-gel synthesis in the presence of a polymeric substrate (polyvinyl alcohol (PVA)) for boron stabilization [13,17].

Compared to dense glasses, mesoporous BGs (MBGs) offer outstanding opportunities for tissue engineering and drug delivery applications [18]. MBGs with well-ordered pores can be obtained when a structure-directing agent (e.g., Pluronic P123) is used in the synthesis process. A wide range of MBG compositions can be produced by changing the glass precursors (type, amount). Indeed, there are more than 10^{52} potential compositions of glasses that can be created by mixing 80 elements discretely at 1 mol% [19,20]; however, only a limited set of dopants is significant for biomedical applications. Various therapeutic elements at defined concentrations have been added to the basic chemical composition of BGs to enhance their physico-chemical, mechanical, and biological performance [21,22]. For instance, cobalt (Co)-containing BGs can promote pro-angiogenic capacity *in vitro* and *in vivo* [23,24]. Copper (Cu)-doped BGs have also been shown to promote angiogenesis and to have higher tissue regeneration potential as well as antibacterial activity compared to Cu-free BGs [25,26]. It is also worth highlighting that copper is cheaper than other antibacterial metals, like silver [27]. Hence, Cu and Co are highly interesting dopants to be incorporated in BGs and their synergistic effects indeed deserve to be investigated; however, there is a paucity of literature about Co/Cu-codoped glasses. Specifically, the syntheses of just a couple of silicate glasses produced by sol-gel (doping with 1 mol.% Co and 1 mol.% Cu) [28] and melt-quenching (doping with 5 mol.% Co and 3 mol.% Cu) [29] have been reported so far.

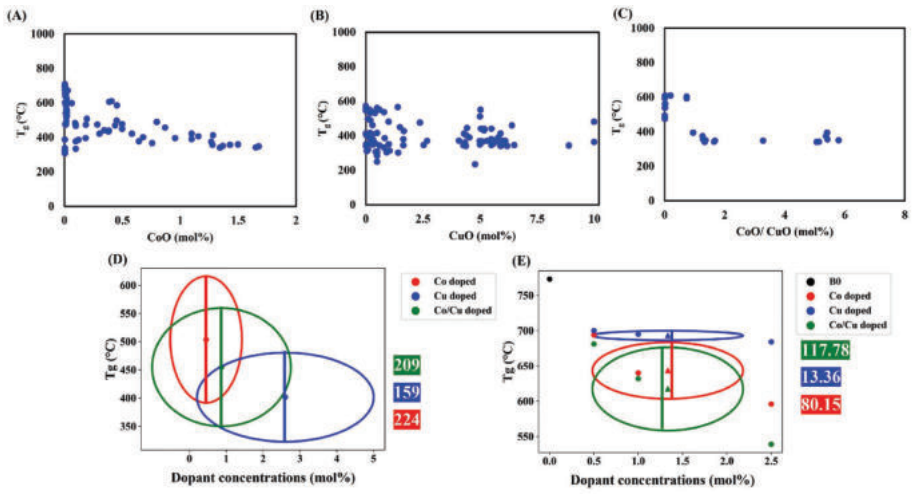

Fig. 1. The correlation between the T_g-compositions in the doped borate glass with (**A**) Co, (**B**) Cu, and (**C**) Co/Cu containing glasses extracted from the SciGlass database. The role of the dopants and their concentration on the T_g of (**D**) the extracted borate glass from the SciGlass database. (**E**) the presentation of experimental data using ellipses. Based on the presentation dopants influence T_g in the following order: Co/Cu > Co > Cu.

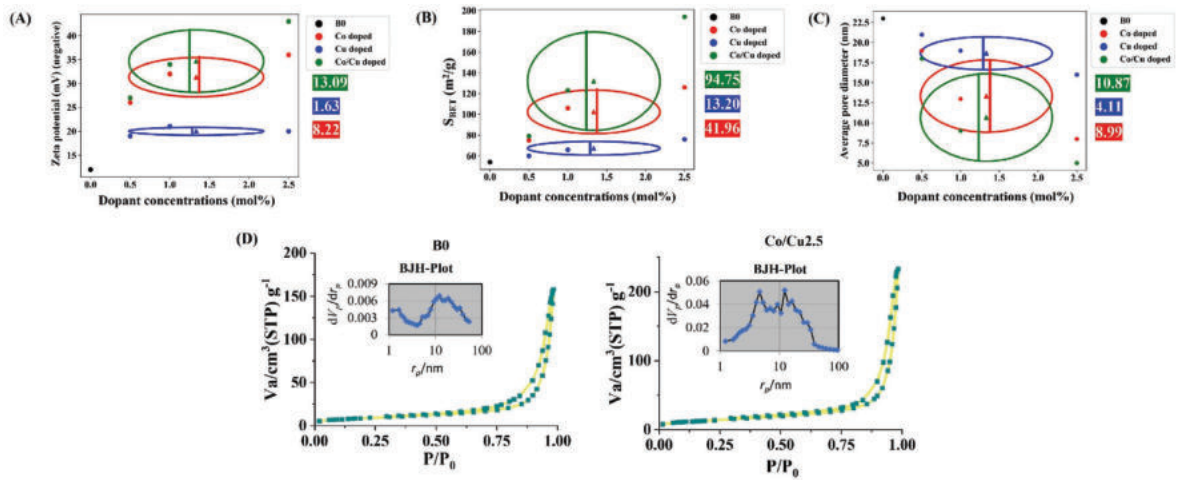

Fig. 2. A presentation of (**A**) zeta potential, (**B**) S_{BET}, and (**C**) average pore diameter data in various MBGs in the form of an ellipse. According to the presentation, the role of dopants on characterization data can be summed up as Co/Cu > Co > Cu in order of importance. (**D**) N_2 adsorption-desorption isotherms and BJH curves of dopant-free (B0) and co-doped samples with 2.5 mol% dopants (Co/Cu2.5).

In the current study, we successfully synthesized a series of MBGs based on the 13-93B3 borate composition in the presence of Pluronic P123 using a modified sol-gel synthesis method. The glasses were doped with various amounts of cobalt (Co^{2+}) and copper (Cu^{2+}) ions alone or simultaneously, taking the total amount of these dopants equal to 0.5, 1, or 2.5 mol%. A complete series of techniques and assays have been employed to determine the physico-chemical and biological properties of the synthesized MBGs. Then, we examined the effects of the synthesis parameters on the physico-chemical characteristics as well as the *in vitro* and *in ovo* properties of MBGs using data science (Python-based data science) to have a better understanding of the obtained experimental data. To the best of the authors' knowledge, this is the first study in which sol-gel mesoporous borate glasses are doped with Cu and Co to provide the 13-93B3 parent glass with improved pro-angiogenic and antibacterial properties for potential use in tissue engineering applications.

2. Materials and methods

2.1. Glass synthesis

In order to synthesize 10 g of the glasses (Table 1), the required amounts of analytical grade raw materials (Samchun Chemical Co., South Korea), including $B(OH)_3$, $Ca(NO_3)_2 4H_2O$, $Co(NO_3)_2 9H_2O$, $Cu(NO_3)\cdot 3H_2O$, $Mg(NO_3)_2 6H_2O$, KNO_3, $NaNO_3$, and $(C_2H_5)_3PO_4$, were first defined using HSC chemistry 9.4 (Outotec®, Espo, Finland). For all the designed systems, the first synthesis step was to dissolve 2 g of P123 (EO_{20}-PO_{70}-EO_{20}, M_W = 5800 g/mol) polymeric template in 100 mL of absolute ethanol in the presence of 0.1 mL of hydrochloric acid (HCL, 37% (w/w)) at 70 °C for 1 h. Afterward, 20 mL of deionized water was added to the solution to dilute and prepare the batch for the next step (the nitrate precursors dissolution). Briefly, the precursors were added separately to the polymeric solution at time intervals of 60 min. Ammonium hydroxide (NH_4OH (25% (w/w)) was added to the final solution to raise the pH to 14, and then the samples were shaken at 70 °C for 5 h. The obtained viscous gels were aged in sealed bottles for 7 days. Following the aging process, the gels underwent a two-step drying process at 70 and 140 °C (24 h for each step). Final heat treatment with a rate of 1 °C/min was carried out on the samples at 550 °C for 24 h.

2.2. Thermodynamic aspects of BGs

Initially, the data of 23,000 borate glass compositions were extracted from the SciGlass database (version 7.12). To assess the relationship between the composition and thermal behavior of glasses, the extracted data were analyzed with SPSS version 18.12 (IBM, USA) in accordance with Eq. (1).

$$\langle aB_2O_3 - bCoO - cCuO - d \mid a = \mathrm{Max}, b \,\&\, c \leq 10 \rangle \qquad \text{Eq. 1}$$

where "a" denotes mol% of B_2O_3, "b" and "c" represent mol% of additives/dopants (Co and Cu, respectively), and "d" is mol% of other components/additives in the glass structure.

2.3. Glass characterizations

To study the thermal properties of the glass gels, differential thermal analysis/thermogravimetric analysis (DTA/TGA) (Bahr STA-503, BAHR, Germany) was performed with a heating rate of 10 °C/min. Zetasizer analysis (NANO-flex® II, Thermo Fisher Scientific, USA) was applied to determine the surface charge of the synthesized MBGs. For this aim, 0.01 g of MBGs was dispersed in absolute ethanol for 10 min with the help of a probe solicitor (Fisher Scientific, USA). Brunauer-Emmett-Teller (BET) and Barrett-Joyner-Halenda (BJH) analyses (ASSP 2020, USA) (N_2 adsorption/desorption analysis) were used to identify the mesoporous characteristics of the glass. For this purpose, the samples were first degassed at 250 °C for 6 h under a vacuum before the analysis. The crystalline phase of the samples was determined using X-ray diffraction (XRD) analysis (D8 Advance, Bruker, Germany). To this end, monochromatic Cu-Kα radiation with a step size of 0.02° and a time per step of 1 s was employed over a 2θ range of 20 to 80°. Rietveld refinement analysis was employed to calculate the lattice constants of the crystalline phase using the Profex package (Graphical Rietveld refinement software, version 5). Field-emission scanning electron microscopy (FESEM) (MIRA3, Tescan, Czech Republic) was utilized to visualize the surface morphology of MBGs before and after soaking in simulated body fluid (SBF). The samples were sputter-coated (Edwards coating system E306A, UK) with gold before analysis.

2.4. Bioactivity assessment

The *in vitro* mineralization process on the synthesized MBGs was assessed by soaking MBGs in SBF. For this purpose, SBF was first prepared in accordance with Kokubo's method [30]. Following this, 0.15 g of each glass was immersed in 100 mL of SBF (mass-to-volume ratio 1.5 mg/mL, as suggested by relevant recent research [31]), and shaken using an orbital shaker (Stuart Orbital Shaker, SI500, UK) for 1, 3, 5, 7, 14, and 21 days. Moreover, inductively-coupled plasma atomic emission

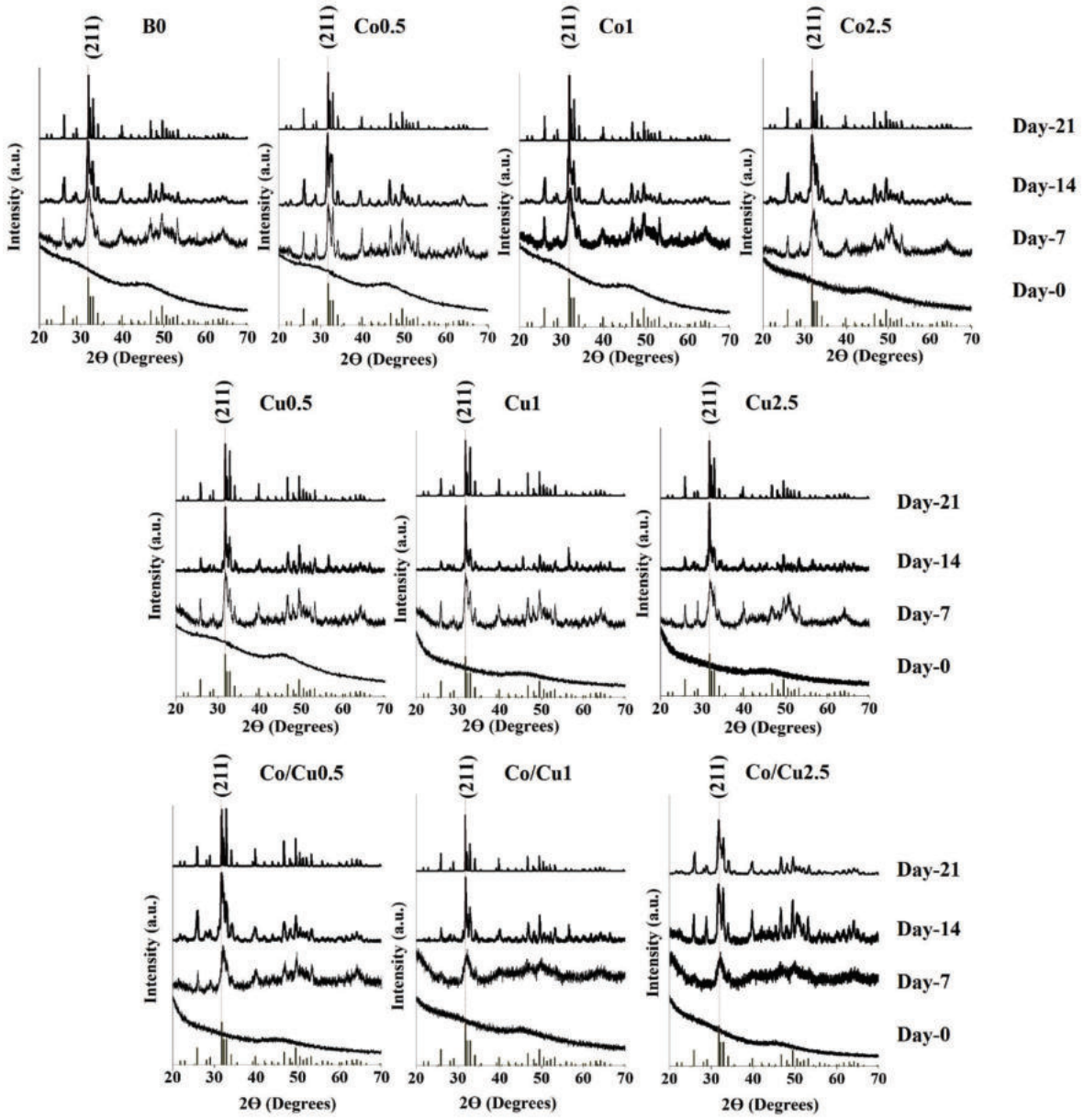

Fig. 3. XRD patterns of the dopant-free and doped MBGs before and after immersion in SBF for 7, 14, and 21 days; major peaks of HAp are visible in all samples at 7, 14, and 21 days.

Table 3
The calculated lattice constant of the borate-based MBGs after 21-day immersion in SBF.

Dopant (mol%)	Co		Cu		Co/Cu	
	a (Å)	c (Å)	a (Å)	c (Å)	a (Å)	c (Å)
0	9.424	6.879	9.424	6.879	9.424	6.879
0.5	9.437	6.881	9.436	6.880	9.440	6.882
1	9.439	6.883	9.434	6.881	9.442	6.883
2.5	9.441	6.883	9.439	6.884	9.444	6.884

spectroscopy (ICP-AES, Spectro Arcos, Kleve, Germany) was applied to measure changes in ion concentrations in the bioactive glass-containing solutions.

2.5. In vitro biocompatibility assessment

2.5.1. Cell viability

The MTT assay was performed on dopant-free and Co-/Cu-doped MBGs using mouse fibroblasts (L929 cell line). First, the cells at a concentration of 3×10^3 cells were seeded in 96-well cell culture plates (SPL Life Science, South Korea) and cultured using Dulbecco's Modified Eagle Medium (DMEM) enriched with 10% v/v fetal bovine serum (FBS) and 1% v/v antibiotic (penicillin/streptomycin) (PAN-Biotech, USA). Afterward, conditioned media were prepared by adding the glass samples to FBS-free DMEM at concentrations of 2 mg/mL. Next, the cells were incubated with the prepared conditioned media for 24, 48, and 72 h. Following these incubations, MTT solution (0.5 mg/mL, Sigma-Aldrich) was added to each well and incubated for another 4 h. After taking out the whole culture media, 100 μL of dimethyl sulfoxide (DMSO, Sigma-Aldrich, USA) was added to each well. Lastly, the cell viability was determined by measuring the optical density (OD) of the different groups at 570 nm and 690 nm with a microplate reader (Epoch, Bio Tek,

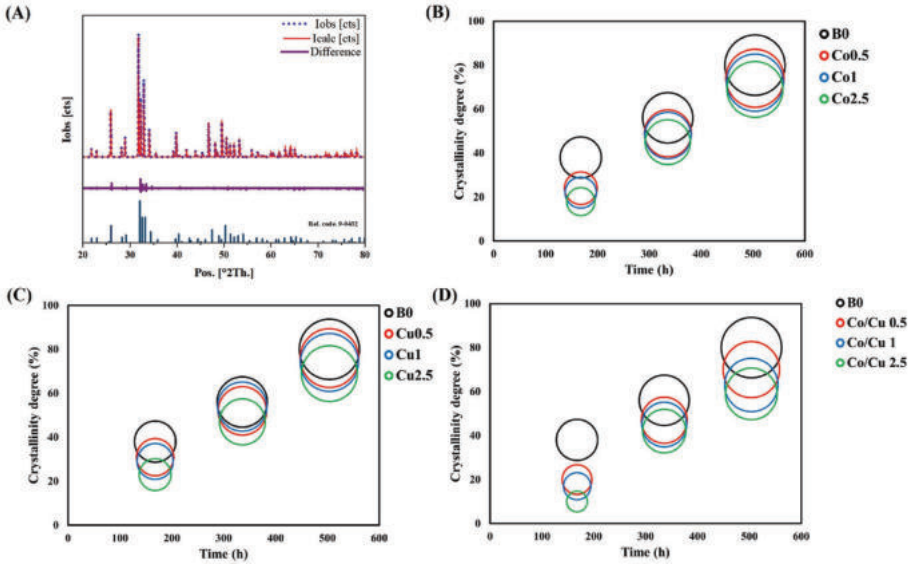

Fig. 4. (**A**) Rietveld refinement pattern of the dopant-free group (B0), including observed (obs), calculated (calc), and difference (obs-calc) intensities. The circle presentation of the crystallinity/time in the immersed (**B**) Co-, (**C**) Cu, and (**D**) Co/Cu-doped MBGs.

Table 4
The crystallinity degree trends of the dopant-free and doped borate MBGs after immersing in SBF.

Dopant (mol%)	Co				Cu				Co/Cu			
	Crystallinity degree (%)				Crystallinity degree (%)				Crystallinity degree (%)			
	7	14	21	Equation	7	14	21	Equation	7	14	21	Equation
0	38	56	80	$y = 0.125x + 16$ $R^2 = 0.9932$	38	56	80	$y = 0.125x + 16$ $R^2 = 0.9932$	38	56	80	$y = 0.125x + 16$ $R^2 = 0.9932$
0.5	24	49	74	$y = 0.1488x - 0.3333$ $R^2 = 0.9979$	31	52	76	$y = 0.1339x + 8$ $R^2 = 0.9985$	17	47	70	$y = 0.1577x - 8.3333$ $R^2 = 0.9942$
1	22	49	72	$y = 0.1488x - 2.3333$ $R^2 = 0.9979$	29	54	74	$y = 0.1339x + 7.3333$ $R^2 = 0.9959$	17	45	63	$y = 0.1369x - 4.3333$ $R^2 = 0.9845$
2.5	18	46	69	$y = 0.1518x - 6.6667$ $R^2 = 0.9968$	23	47	69	$y = 0.1369x + 0.3333$ $R^2 = 0.9994$	10	42	59	$y = 0.1458x - 12$ $R^2 = 0.9697$

US).

2.5.2. Blood compatibility test

For this purpose, blood from three healthy volunteer women was collected under the ethical approval of the Mashhad University of Medical Sciences (IR.MUMS.MEDICAL.REC.1400.453). To prevent clotting, sodium citrate was used as an anticoagulant agent on fresh blood. Then MBGs were added to the blood samples (2 mg/mL) and incubated at 37 °C for 60 min. A negative control was diluted blood in normal saline, and a positive control was diluted blood in deionized water. An Epoch microplate reader (BioTek, US) was used to read the OD of collected supernatants after centrifugation of the samples at 1500 rpm for 10 min. In order to calculate the amount of hemolysis, we used the following formula (**Eq. 2**) [32]:

$$\text{Hemolysis}\ (\%) = \left[\frac{D_s - D_n}{D_p - D_n}\right] \times 100 \qquad \text{Eq. 2}$$

where the absorption of samples, the positive control, and the negative control were represented by D_s, D_p, and D_n, respectively.

2.5.3. Cell attachment study

To evaluate the cell adhesion onto the prepared glasses, a pellet of the samples with (diameter of 5 mm and thickness of 1 mm) was first prepared by using a hydraulic press (Endecott Ltd, London, UK) with a 1-ton load. Then $3x10^3$ mouse fibroblasts (L929 cell line) were seeded onto the pellets. Following 72 h of incubation, the cell-laden samples were fixed by immersing in glutaraldehyde 2.5% (v/v) (Merck, Germany) for 24 h. The cell/glass samples were then washed with PBS and dehydrated in increasing concentrations of ethanol (Merck, Germany) (30%, 45%, 50%, 60%, 75%, 80%, 90%, 95%, and 100%). Finally, the samples were freeze-dried for 24 h and sputter-coated with gold before SEM observation.

2.6. Angiogenic activity of MBGs

2.6.1. Scratch assay

Human umbilical vein endothelial cells (HUVECs) were purchased from the National Cell Bank (Pasteur Institute of Iran). HUVECs were seeded in 12 well plates (SPL Life Sciences, South Korea) and cultured with DMEM/Nutrient Mixture F12 (1:1) supplemented with 5% FBS and 1% penicillin/streptomycin (PAN-Biotech, USA). Then a scratch was created in the confluent monolayer of the cells by a 100 μL pipette tip. An inverted microscope (Eclipse TS-100, Nikon, Japan) was used to observe the cell mobility after 24 h of the scratching process. ImageJ software (National Institutes of Health, Bethesda, MD, USA) was utilized to quantify the cell migration process.

2.6.2. In ovo angiogenesis assay

The chick chorioallantoic membrane (CAM) assay was employed to assess the angiogenic potential of the dopant-free and Co-/Cu-doped MBGs *in ovo*. A total of 30 fertilized Leghorn chicken eggs (Tookatalaei, Mashhad, Iran) were used for this assay. First, we cleaned the eggshells with sterile deionized water. The eggs were then incubated for 10 days

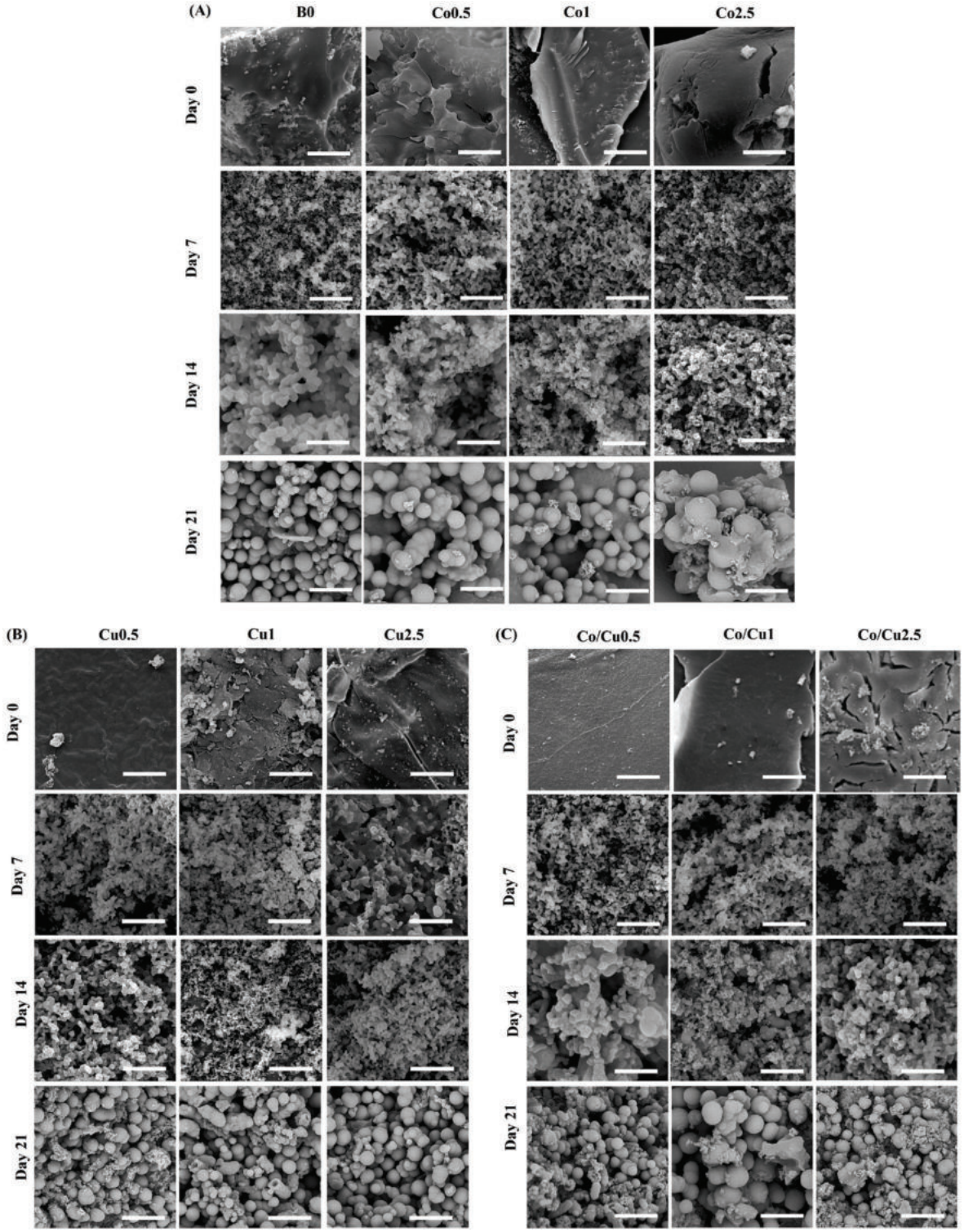

Fig. 5. SEM micrographs of (**A**) doped MBGs with Co, (**B**) doped MBGs with Cu, and (**C**) co-doped MBGs with Co/Cu before and after immersing in SBF (scale bar = 2 μm).

at 37 °C in 70% humidity. After that, a square window (approximately 1.5 cm diameter) was created on the upper side of the eggs. The MBG pellets (diameter of 5 mm and thickness of 1 mm) were first sterilized by holding them at 160 °C for 30 min (following the procedure reported in Ref. [33]) and then placed on the intact CAM. The eggs without the glasses were considered the control samples. Images were taken after 3 days of incubation, and the results were analyzed using ImageJ software (National Institutes of Health, Bethesda, MD, USA).

2.7. Antibacterial activities

The antibacterial activity of dopant-free and Co-/Cu-doped MBGs was examined against Gram-negative *Pseudomonas aeruginosa* (*P. aeruginosa*) and Gram-positive *Staphylococcus aureus* (*S. aureus*). The bacteria were cultured in a lysogeny broth (LB) medium at 37 °C for this purpose. After sterilization, the MBGs (2 and 4 mg/mL) were added to LB and incubated at 37 °C for 24 h. The glass-containing media were

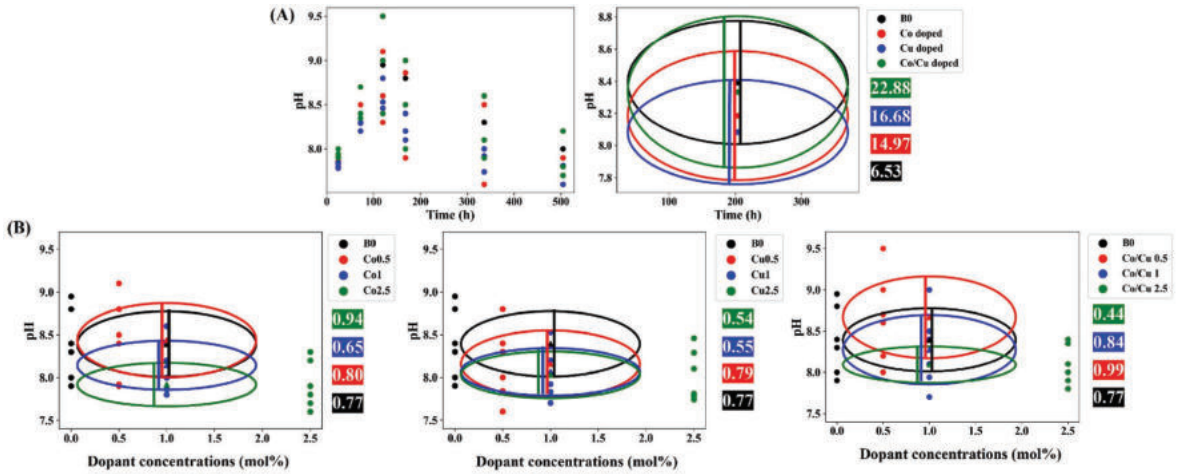

Fig. 6. (A) Profile and (B) ellipse presentation of pH changes during 21 days.

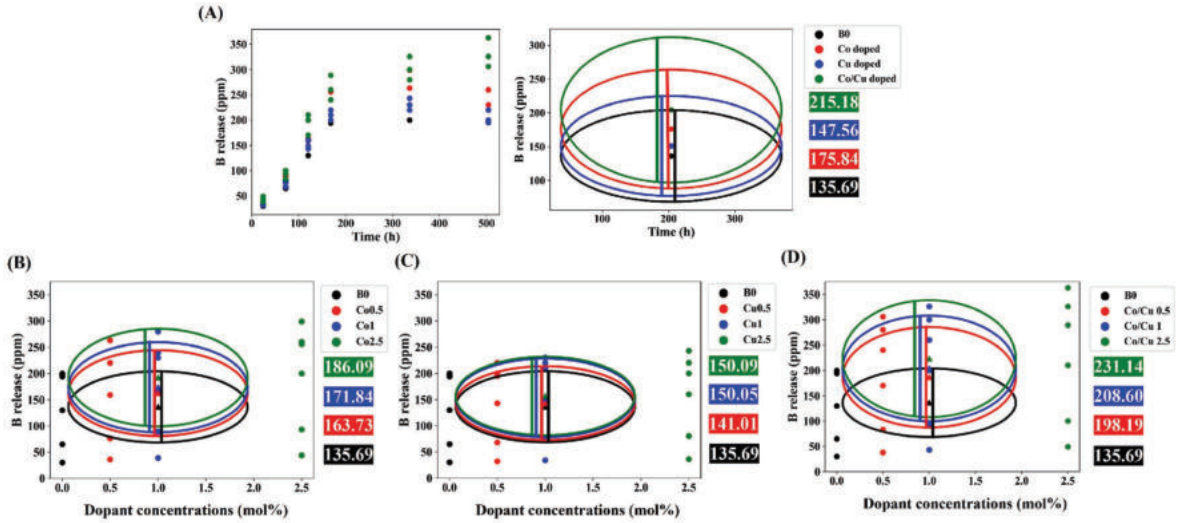

Fig. 7. (**A**) B^{3+} ions release-time profile, the role of (**B**) Co-, (**C**) Cu, and (**D**) Co/Cu on the release of B^{3+} ions.

then added to the 1–5 × 10^5 CFU/mL bacterial suspension and incubated at 37 °C for 24 h. Samples without MBGs were considered the control groups. The OD of the media was measured using microplate readers (Epoch, Bio Tek, US) at 600 nm. The antibacterial activity of the glass samples was calculated using **Eq.** 5 [34]:

$$\text{Antibacterial activity } (\%) = \left(D_s \,/\, D_p\right) \times 100 \qquad \text{(Eq. 5)}$$

where D_s and D_p mean the absorption of a bioactive glass-treated bacteria and the control, respectively.

In the following assay, a uniform layer of LB agar was spread on a Petri dish (diameter 10 cm^2). As described above, the MBG pellets with a diameter of 5 mm and a thickness of 1 mm were prepared using a hydraulic press (Endecott Ltd, London, UK) and then placed in a Petri dish containing Gram-negative *P. aeruginosa* and Gram-positive *S. aureus* bacteria for 24 h. The inhibition zones were analyzed using ImageJ software (National Institutes of Health, Bethesda, MD, USA). MBGs were also investigated for their antibacterial activity using the colony forming unit (CFU) method. To do this, 2 mg/mL of MBGs was first incubated in the nutrient broth inoculated with *P. aeruginosa* and *S. aureus* at 37 °C for 48 h. Then, the supernatant was collected and incubated with both bacterial strains for 24 h. Afterward, 50 μL aliquots of each solution were spread over agar plates and incubated at the same conditions for 24 h. In the end, colonies were counted.

2.8. Statistical analysis

The biological experiments, including the *in vitro* biocompatibility assessments, antibacterial activity test, and angiogenesis assays, were carried out at least three times, and the results are reported as mean ± standard deviation (SD). GraphPad Prism (version 9.4.1(681), USA) was used to analyze the data using a one-way ANOVA variance model followed by post-hoc analysis.

2.9. Data analysis

All physicochemical and biological data were processed using Python 3.11 employing Visual Studio Code as an Integrated Development Environment (IDE). K-means algorithms were applied to cluster the data. Following the data processing, innovatively, various ellipses were used to illustrate the effect of dopant type and concentration on the physicochemical and biological properties. In each ellipse, the semi-major and semi-minor axis is related to the SD of the X and Y axis, respectively.

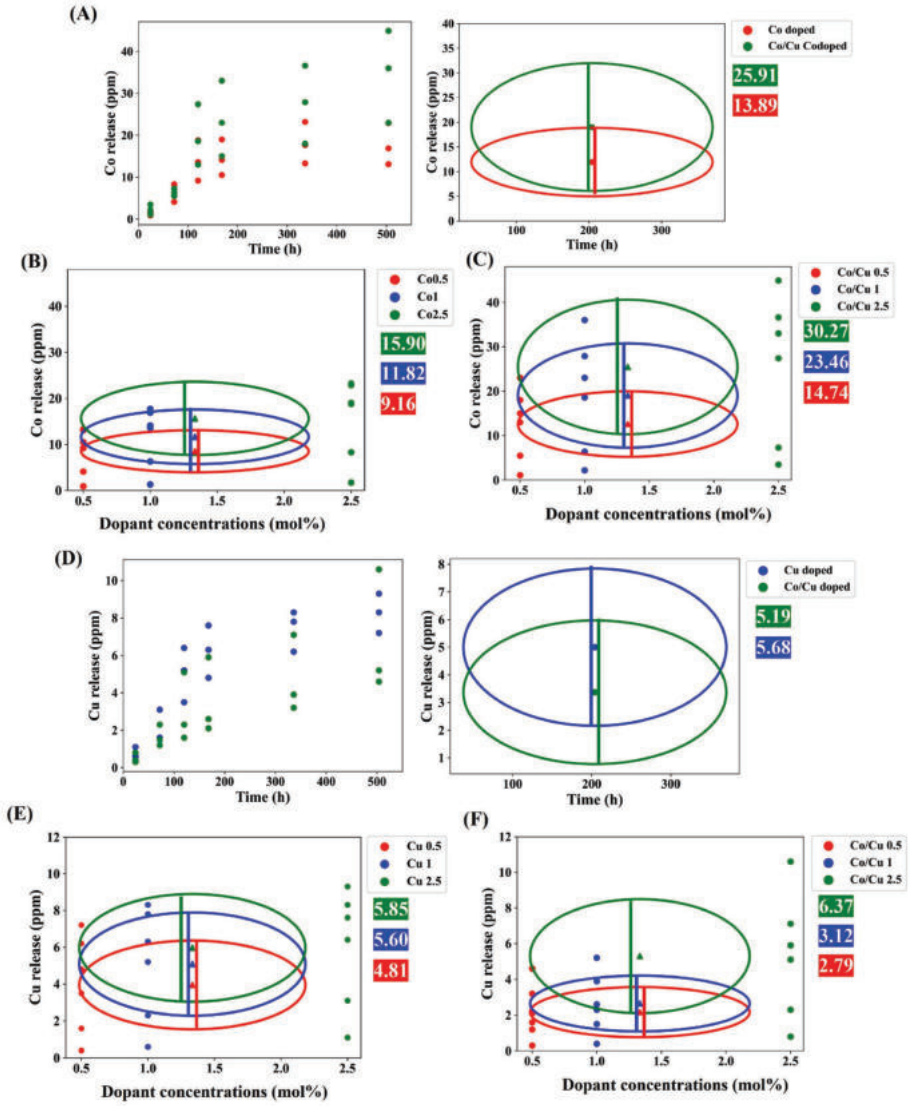

Fig. 8. (A) Time profile for the release of the Co^{2+} ions, and the effect of (B) Co- and (C) Co/Cu on the release of Co^{2+} ions. (D) Time profile for the release of the Cu^{2+} ions, and the effect of (E) Cu- and (F) Co/Cu on the release of Cu^{2+} ions.

3. Results

3.1. Physico-chemical properties

The results of the assessment of T_g, zeta potential, S_{BET}, and average pore diameter of the fabricated glasses are presented in Table 2. The effect of Co, Cu, and Co/Cu dopants on the T_g of extracted borate glass data from the SciGlass database is shown in Fig. 1A-C. According to graphs A-C, the addition of Co, Cu, and Co/Cu dopants to the glass network decreased the T_g of the borate-based glasses. In general, this trend is consistent with theoretical expectations as Co and Cu act as modifiers in the glass network. Based on the ellipse presentation, graph D shows that CoO has a greater impact on decreasing the T_g of adapted data than CoO. Moreover, T_g is found to be more sensitive to co-doped groups than to their single-doped counterparts according to graph D. Experimental data demonstrated a reduction in T_g in Co-doped glasses from 773 °C (B0) to 596 °C (Co2.5). In the doped MBGs with Cu, the T_g values were reduced up to 684 °C (Cu2.5). Furthermore, in the co-doped MBGs, T_g was significantly lower than in single-doped groups. The T_g was reduced to 539 °C for the Co-/Cu-doped samples (Co/Cu2.5).

The zeta potential values of the doped MBGs decreased from -12 (B0) to -36 (Co2.5), -20 (Cu2.5), and -43 mV (Co/Cu2.5). Fig. 2A presents an ellipse representation of the effect of dopants on the zeta potential of the MBGs. The ellipse shows that dopants affect zeta potential in the following order: Co/Cu > Co > Cu. This trend is analogous to that already observed for T_g.

The results of the BET/BJH analyses indicated that the dopants play a significant role in the mesoporous characteristics of MBGs. The S_{BET} of the doped MBGs was significantly increased from 54 m^2/g (B0) to 126 (Co2.5), 76 (Cu2.5), and 194 m^2/g (Co/Cu2.5). A decreasing trend in the pore diameter was recorded from 23 nm (B0) to 8 nm (Co2.5), 16 nm (Cu2.5), and 5 nm (Co/Cu2.5). The ellipse presentation of S_{BET} and pore diameter data clarifies the role of dopants on the mesoporous characteristics (Fig. 2B and **C**). In addition, N_2 adsorption-desorption isotherms and BJH curves of dopant-free (B0) and co-doped samples with 2.5 mol % dopants (Co/Cu2.5) are shown in Fig. 2D. Based on the International Union of Pure and Applied Chemistry (IUPAC) classification, the glass isotherms can be considered as category IV, confirming the mesoporous nature of the particles. This is consistent with BJH results revealing a mesoporous range.

The XRD patterns of the synthesized MBGs before and after soaking in SBF are displayed in Fig. 3A. The graph confirmed the amorphous state of the synthesized samples before immersion in SBF (day 0). After 7 days of incubation in SBF, a hydroxyapatite (HAp, Ref. code. 9-0432)-

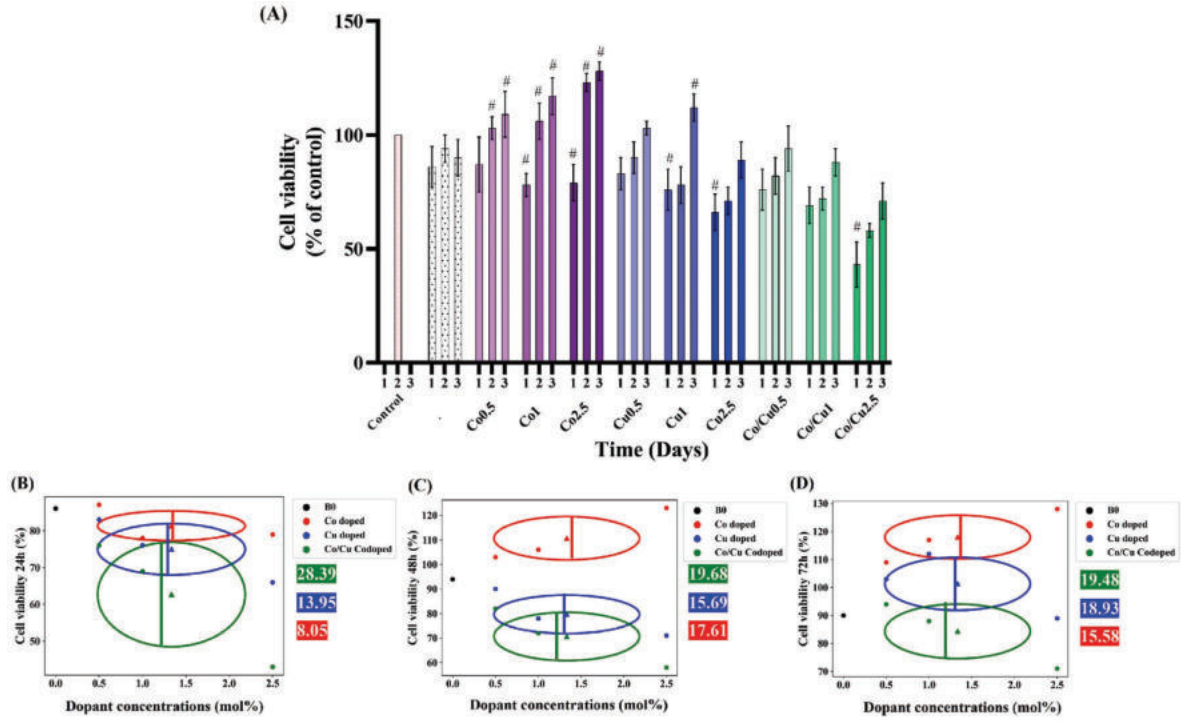

Fig. 9. (A) The MTT results of treated L929 cells with MBGs. The MTT data are in ellipse format after (B) 1, (C) 2, and (D) 3 days. The statistically significant differences were marked based on the p-values (#$p \leq 0.05$). (# Indicate comparison with the control).

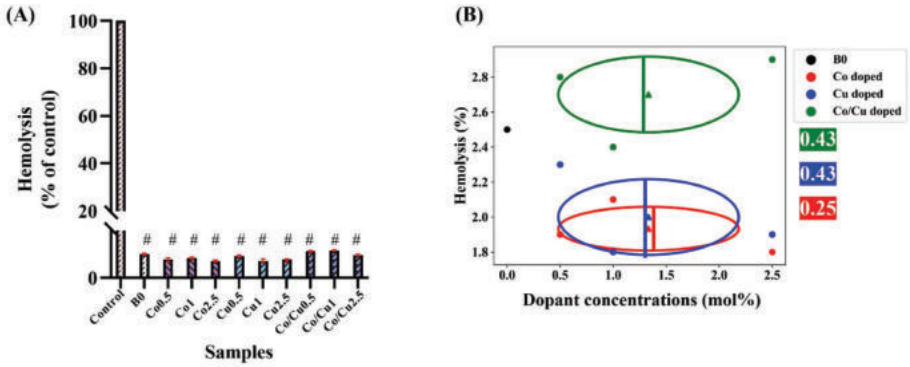

Fig. 10. The effect of the different compositions of the borate glasses on the red blood cells (**A**) and ellipse presentation of the hemolysis data (**B**). The statistically significant differences were marked based on the p-values (#$p \leq 0.05$). (# Indicate comparison with the control). (For interpretation of the references to colour in this figure legend, the reader is referred to the Web version of this article.)

like layer is formed onto all MBGs. A significant increase in the crystallinity of HAp was observed during the immersion of MBGs in SBF (Table 3). Rietveld refinement analysis was used to calculate the lattice constants of crystalline HAp, as shown in Table 3 and Fig. 4A. According to the Rietveld data, the lattice constants of HAp (a = 9.424 Å, c = 6.879 Å) increased to (a = 9.441 Å, c = 6.883 Å), (a = 9.439 Å, c = 6.884 Å), and (a = 9.444 Å, c = 6.884 Å) in the doped MBGs with 2.5 mol% of Co (Co25), Cu (Cu2.5), and Co/Cu (Co/Cu2.5), respectively. After 21 days, the crystallinity degree of HAp formed on the Co/Cu-free MBG reached 80%; this value decreased to 69, 69, and 59% for MBGs doped with 2.5 mol% of Co, Cu, and Co/Cu, respectively, at the same time point. A circle representation was used to illustrate the trend of increasing crystallinity degree of different groups (Fig. 4B-D). A linear equation is presented in Table 4 based on these circle representations. Based on crystallinity data, doped MBGs exhibit a faster rate of crystallinity increase (the slope of equations) than those without dopants (B0).

A series of SEM micrographs of the fabricated MBGs before and after immersion in SBF is shown in Fig. 5A-C. The synthesized MBGs before immersion in SBF have irregular shapes. The mineralization of HAp on the bioactive glass surface was detected after 7 days of SBF incubation; the nucleated HAp has grown following the elapsed time period. Eventually, all the samples were mineralized with a globular morphology, which is typical of HAp, after 21 days. The size of HAp crystals increased over time, in accordance with the XRD results (the diffraction peaks of the newly formed phase progressively become sharper and narrower).

3.2. pH profile

Fig. 6A shows the pH changes for the SBF-immersed MBGs. The pH values reached their maximum after five days of immersion; specifically, the recorded pH peaks were 9.1, 8.8, and 9.5 for the dopant-free, Co-, Cu-, and Co-/Cu-doped samples, respectively. According to Fig. 6B (the ellipse profile of pH), the effect of dopants on the pH follows the trend Co/Cu > Co > Cu, which is also consistent with that observed for the

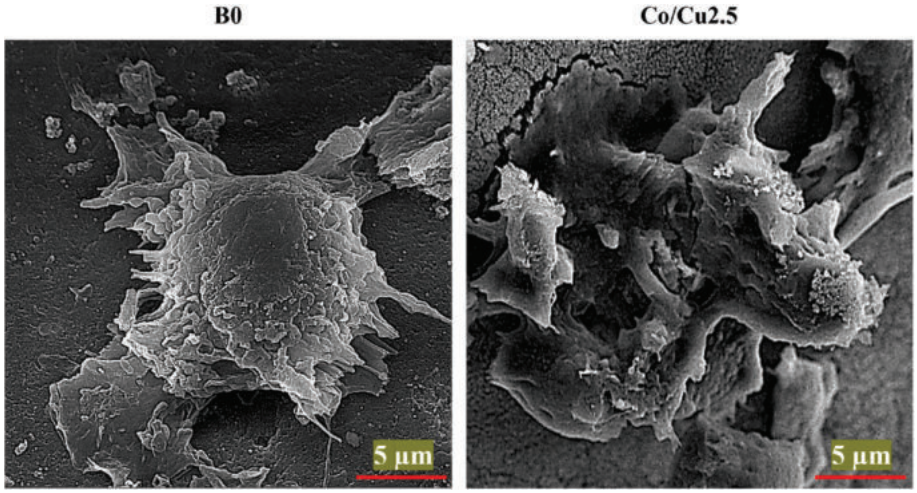

Fig. 11. L929 cell attachment onto the 13-93B3 borate glasses, including (A) dopant-free and (B) 2.5 mol% Co/Cu-doped MBGs.

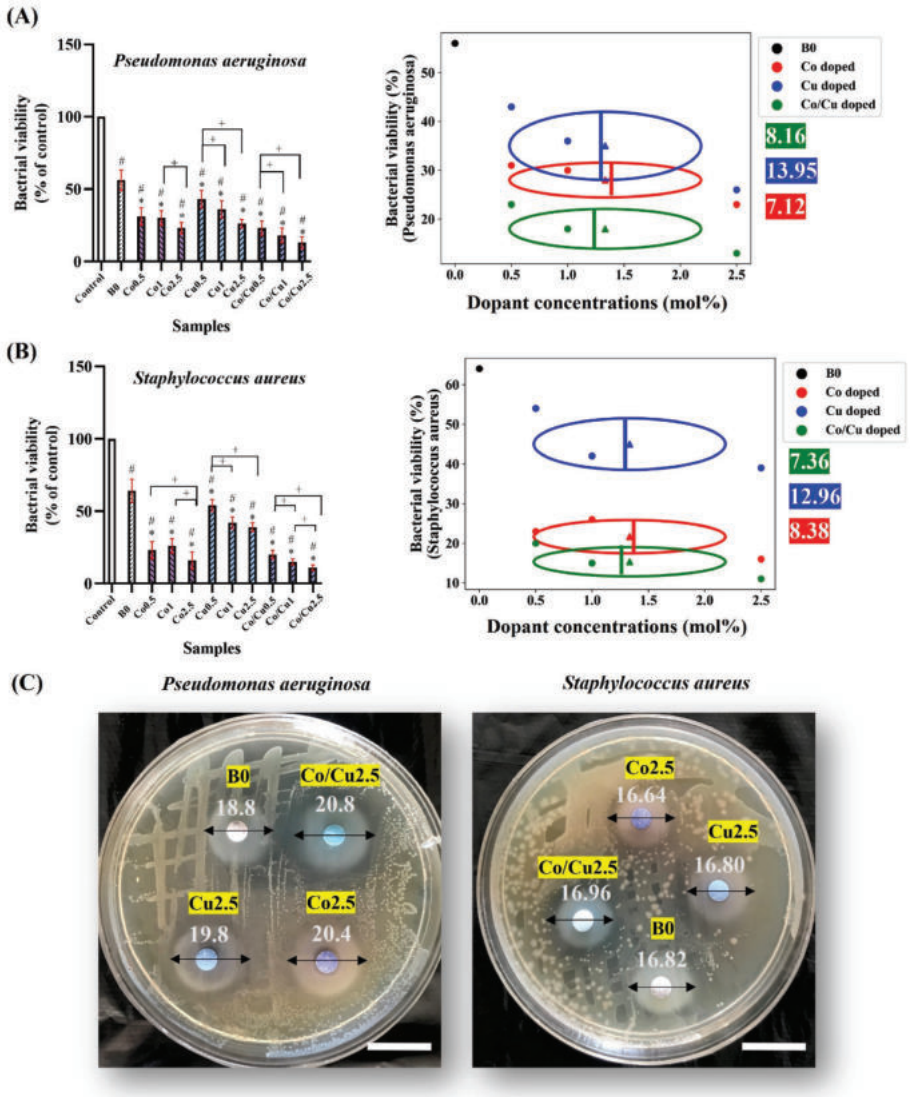

Fig. 12. The viability results and ellipse representation of (**A**) Gram-positive and (**B**) Gram-negative bacteria treated with MBGs. (**C**) The inhibition zones of the MBG pellets against Gram-positive and Gram-negative bacteria (scale bar = 20 mm). The statistically significant differences were marked based on the p-values (#, *, and + $p \leq 0.05$). # and * indicate the comparison with control and B0, respectively, and + shows the comparison between the doped samples in each group.

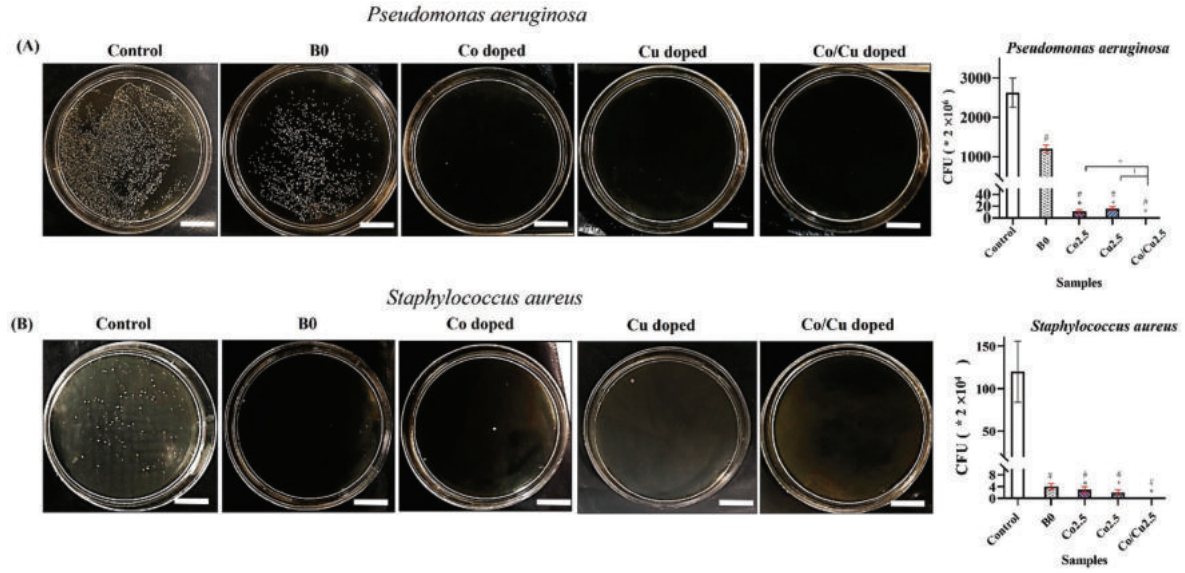

Fig. 13. The CFU results of (**A**) Gram-positive and (**B**) Gram-negative bacteria treated with MBGs. (scale bar = 1 cm). The statistically significant differences were marked based on the p-values (# and * $p \leq 0.05$). # and * indicate the comparison with control and B0, respectively.

properties collected in Table 2. Additionally, increasing the dopant concentration up to 0.5 mol% led to an increase in the pH values, while increasing the dopant concentration between 1 and 2.5 mol% resulted in a decrease in the pH values.

3.3. Ion release profile

3.3.1. Boron release profile

The release profile of boron (B) from the prepared MBGs is displayed in Fig. 7A. According to the profiles, the concentration of B increased continuously in both dopant-free and single-doped groups (Co- and Cu-doped) over 14 days. However, the B concentration in these groups showed a decreasing trend over 14-21 days. A continuous increase in B^{3+} ions concentration is observed in co-doped MBGs over 21 days. The highest measured B^{3+} ion concentrations for dopant-free, Co-, Cu-, and Co/Cu-doped groups were 200 (B0-14 days), 299 (Co2.5-14 days), 243 (Cu2.5-14 days), and 363 ppm (Co/Cu2.5-21 days). As illustrated by the ellipse of Fig. 7B-D, Co-/Cu-doped borate 1393B3 glasses release the B^{3+} ions more than their single-doped (Co- and Cu-doped) counterparts.

3.3.2. Co and Cu release profile

Fig. 7A-C displays the ellipse representation of the Co ion release profile in the Co-doped MBGs. Data indicated that the highest concentrations of the Co^{2+} ions were 22.9 (Co2.5) and 44.9 ppm (Co/Cu2.5) after 21 days. Considering the data and ellipse representation, it appears that single-doped MBGs release less Co^{2+} than co-doped MBGs (Co-/Cu-doped glasses).

Fig. 7D-F shows the release profiles of the Cu^{2+} ions in Cu-containing MBGs with their ellipse representations. Based on the data, the highest concentration of the Cu^{2+} ions were 9.3 (Cu2.5), and 10.6 ppm (Co/Cu2.5). Data and ellipse representations have shown that Cu^{2+} release in Cu-containing MBGs with 0.5 and 1 mol% is greater than Co/Cu-doped counterparts. Additionally, the release of Cu^{2+} in co-doped MBGs with 2.5 mol% dopants is higher than in single-doped counterparts.

3.4. Biological performance of MBGs

3.4.1. Cell viability

The viability of L929 cells treated with MBGs is illustrated in Fig. 9A. In accordance with the data, MBGs reduced the viability of the cells after 24 h, especially in Co1 (78%) Co2.5 (79%) Cu1 (76%) Cu2.5 (66%), and Co/Cu2.5 (43%) ($p < 0.05$). However, the cell viability showed a significant improvement after 72 h treatment with the glasses, especially in the Co0.5 (109%), Co1 (117%), Co2.5 (130%), and Cu1 (112%) groups ($p < 0.05$). An ellipse representation in Fig. 9B-D illustrates how dopant type can affect cell viability over time.

3.4.2. Blood compatibility

The results of the blood compatibility test are displayed in Fig. 10A. Compared to the positive control (hemolyzed blood in the presence of distilled water), no significant hemolysis effect was observed for the glass samples ($p < 0.05$). Fig. 10B shows the ellipse representation of the dopant role in hemolysis as follows: Co/Co > Cu > Co.

3.4.3. Cell attachment

Fig. 11 shows the SEM micrographs of the dopant-free sample and MBGs doped with 2.5 mol% Co/Cu seeded with L929 cells. According to these images, it can be stated that L929 cells can attach to and expand onto the glass samples.

3.4.4. Antibacterial activity

Fig. 12A and **B** shows the bacterial vitality of *Pseudomonas aeruginosa* (Gram-negative) and *Staphylococcus aureus* (Gram-positive) treated with MBGs. Data analysis demonstrated that all MBG-treated bacteria had lower viability compared to the control ($p < 0.05$). It appears that the Co/Cu-doped MBG groups had a greater effect on reducing bacteria viability than their single-doped counterparts according to the data and ellipse presentation. Gram-negative and Gram-positive bacteria had the lowest viability of 13 and 11% for co-doped MBGs with 2.5 mol% (Co/Cu2.5). By comparing the data of Co- and Co/Cu-doped MBGs, it can be observed that Gram-negative bacteria are more resistant (up to 25%) against them. Nevertheless, the Gram-positive bacteria in the Cu-doped MBGs groups show higher viability (up to 20%) than the Gram-negative bacteria. The inhibition zones around MBG pellets are shown in Fig. 12C. The zone diameter of Co/Cu2.5 MBGs is 20.8 mm against Gram-positive bacteria and 16.96 mm against Gram-negative bacteria, respectively. Furthermore, as shown in Fig. 13, MBGs effectively inhibited the growth of bacterial colonies. Specifically, it was observed that the co-doped MBGs fully inhibited the growth of both Gram-negative and Gram-positive bacteria.

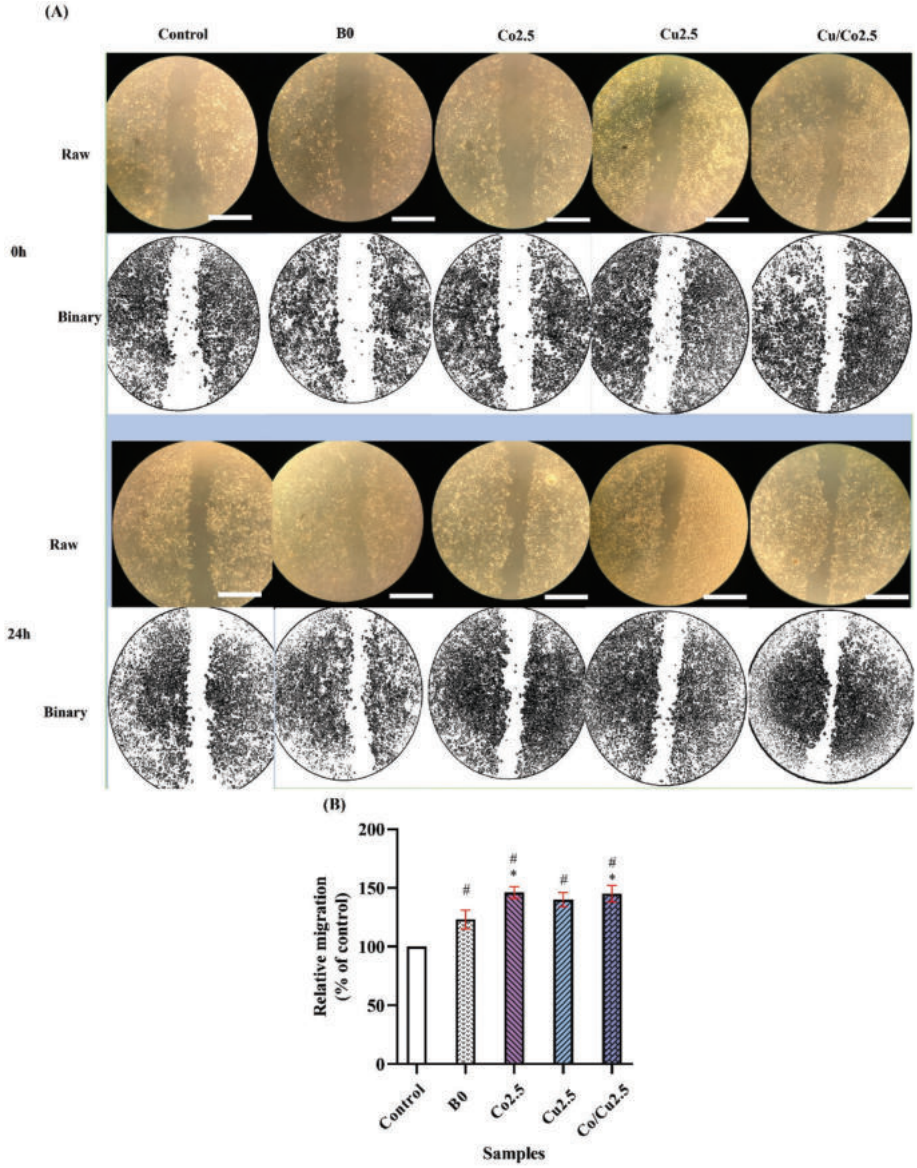

Fig. 14. The migration of HUVECs treated with the dopant-free and Co-/Cu-doped MBGs. (A) Optical microscope images (scale bar: 100 μm). and (B) the quantitative results. The statistically significant differences were marked based on the p-values (# and * $p \leq 0.05$). # and * indicate comparison with control and B0, respectively.

3.4.5. Angiogenesis evaluation

3.4.5.1. In vitro scratch migration assay. *In vitro* HUVECs migration after treatment with MBGs is visualized optically in Fig. 14A. Fig. 14B shows that cell migration significantly increased up to 23, 46, 40, and 45% for dopant-free (B0), doped MBGs with 2.5 mol% Co (Co2.5), Cu (Cu2.5), and co-doped MBGs (Co/Cu2.5) compared to control, respectively. According to statistical analysis, there was no significant difference in migration among cells treated with doped MBGs.

3.4.5.2. In ovo assay. Digital images of the *in ovo* angiogenesis assay are shown in Fig. 15A. The image processing data are also presented in Fig. 15B. Data revealed that vascular density increased up to 12, 23, 14, and 31% for dopant-free (B0), doped MBGs with 2.5 mol% Co (Co 2.5) and Cu (Cu2.5), and co-doped MBGs (Co/Cu2.5) compared to controls, respectively. The statistical analysis indicates that all changes in the angiogenesis of the doped MBGs are significant.

3.5. Data clustering

MBGs were clustered by K-means algorithms based on their physicochemical and biological properties, as shown in Fig. 16. MBGs in the study (10 samples) with a similar weight of 10% were considered in this clustering. In Fig. 16, five independent groups were identified based on the results, including cluster I-10% (B0), cluster II-10% (Co/Cu2.5), cluster III-20% (Co1 and Co2.5), cluster IV-20% (Co/Cu0.5 and Co/Cu1), and cluster V-40% (Co0.5, Cu0.5, Cu1, and Cu2.5).

4. Discussion

Using data science combined with materials science and engineering principles, optimal biocompatible substances can be synthesized for medical purposes. Despite the importance and increasing development of new formulations for tissue repair and regeneration, it is unclear how therapeutic dopants affect the structure and biological behaviors of borate BGs such as 13-93B3 BGs. The discovery and optimization of novel materials are often based on Edisonian "trial-and-error" processes

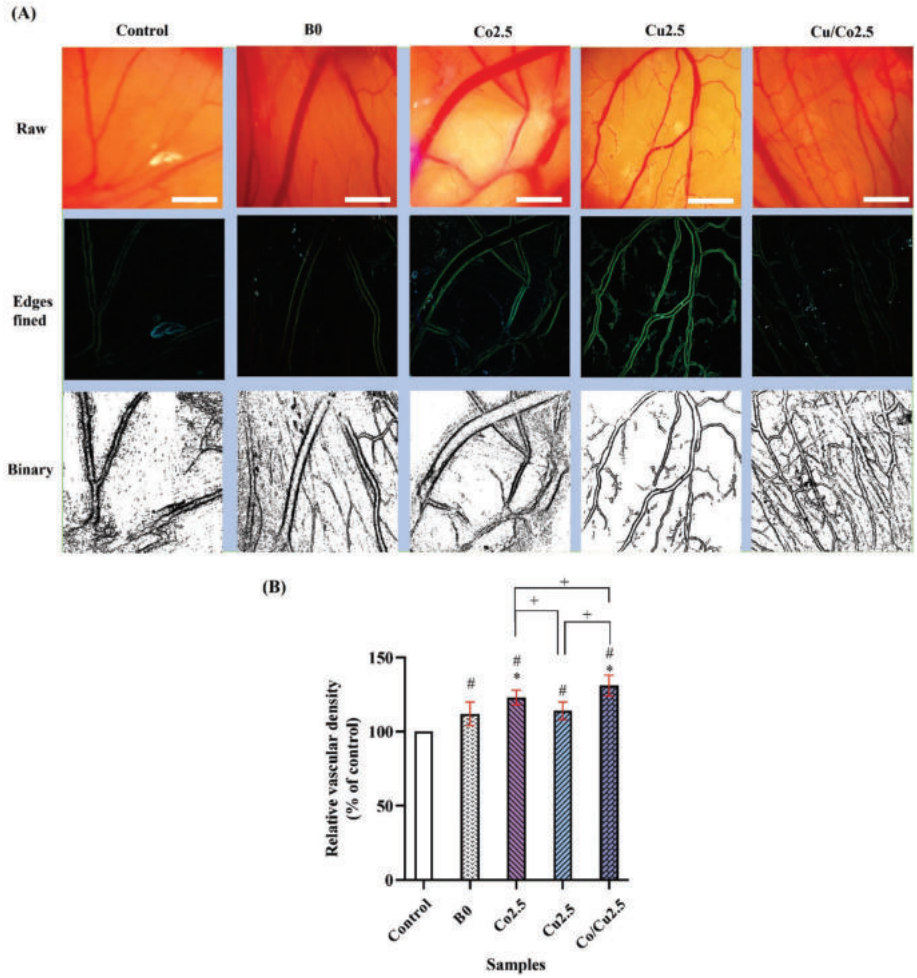

Fig. 15. The effect of the 13-93B3 borate glasses on angiogenesis based on the CAM assay after 3 days of incubation. (A) Digital images (scale bar: 20 mm) and (B) the quantified results of (A). The statistically significant differences were marked based on the p-values (#, *, and + $p \leq 0.05$). # and * indicate comparison with control and B0, respectively, and + shows comparison between the doped samples.

Cluster	Cluster mean				
	Cluster-1	Cluster-2	Cluster-3	Cluster-4	Cluster-5
Tg (°C)	773	539	681	623	693
Zeta potential (mV)	12	43	27	34	21
S_{BET} (m^2/g)	54	194	79	118	69
Bacterial viability (%) (Pseudomonas aeruginosa)	56	13	23	24	34
Cell viability 72 h	90	71	122	91	103
Hemolysis (%)	2.5	2.9	2.8	2.1	1.9
Bacterial viability (%) (Staphylococcus aeruginosa)	64	11	20	19	39
Average pore diameter (nm)	23	5	18	10	19

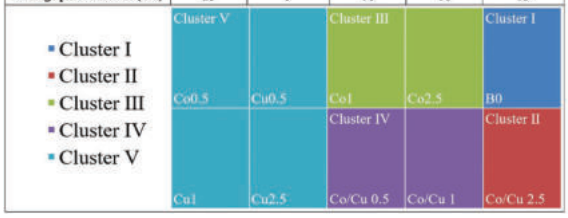

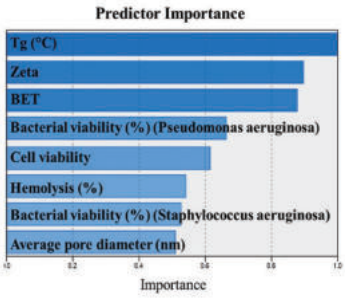

Fig. 16. The results of data clustering of MBGs based on the physicochemical and biological properties of MBGs, including the cluster and predictor importance of the results.

[7]. These materials, however, are easier to discover, optimize, and truly understand when using artificial intelligence and machine learning. In this study, a series of formulations of 13-93B3 borate glasses (see Table 1) were synthesized in the presence of Pluronic P123, which led to obtaining MBGs with well-ordered pores structures. Metal therapeutic ions Co^{2+} and Cu^{2+} were added to the basic composition of 13-93B3 MBGs to enhance their angiogenic and antibacterial properties. We applied data science techniques to provide a deeper understanding of each experimental section.

Co^{2+} ions are an essential component of vitamins B12 and cobalamin, but excess levels of cobalt can adversely affect the nervous, respiratory, and cardiovascular systems [23]. It is believed that the side

effects of cobalt are caused by the release of persistent Co^{2+} ions over time, which may not happen once it is used temporarily. Copper is involved in a wide range of physiological functions in humans. Copper is another excellent element for applications such as implant coatings, biodegradable fillers, and soft/hard tissue healing due to its remarkable antibacterial and angiogenic properties [35].

In borate glasses, ion doping may affect oxygen packing density (OPD), bond length, the concentration of non-bridging oxygens (NBOs), ion mobility, configurational entropy (S_{Conf}), and boron-boron separation [8,36,37]. The modification of the glass network can allow the formation of M-O-B covalent bands (where M is the dopant cation), the formation of bridge networks between [BO_3] and [BO4] units, and the modification of B-O rings and chains with modifier cations (Co^{2+}, Cu^{2+}) [38,39]. As a result of these changes, the glass structure and network distortion are enhanced. The DTA results (Table 2) showed that adding dopants to the basic composition of the glasses leads to a decrease in the T_g of the samples from 773 °C (B0) to 596 (Co-doped), 684 (Cu-doped), and 539 °C (Co-/Cu-doped). Based on the ellipse representation of Fig. 1, increasing the concentration of the dopants from 0.5 to 2.5 mol% results in a decrease in the Tg due to the higher network-modifying role of the dopants. Compared to Cu^{2+} ions, the Co^{2+} ions have a greater influence on the T_g of the glasses which can be due to the higher bond length of Co-O (cation radius of 200 p.m.) in comparison with a lower bond strength of Cu-O (cation radius of 140 p.m.). Co-/Cu-doped MBGs with more complex structures, lower bond strength of glass former, a higher concentration of NBOs, and lower OPD show a lower T_g than single-doped MBGs (Co- or Cu-doped glasses).

In Table 2, the zeta analysis results indicate an increase in the zeta potential value (from -12 to -43 mV) in the case of co-doped MBGs (Cu/Co2.5). The gradient distribution of the dopants on the glass surface could also affect the surface charge [40]. A continuous and concurrent increase in the surface charge is obvious in the ellipse representation once the concentration of dopants was increased (Fig. 2). In response to the increased dopant concentration, the ions "disturb" the glass network, and hence higher repulsion force between the glass particles and decreased agglomeration can occur [41,42]. Furthermore, Co^{2+} ions play a greater role in the zeta potential than Cu^{2+} ions which may be associated with their larger ionic radius. It is important to note that the high surface charge values may improve biological performance, especially during the first stage of cellular reactions [43]. The mesoporous nature of the un-doped and doped MBGs was confirmed by using BET/BJH analysis (Fig. 2). The data from the BET (Table 2) revealed that the S_{BET} of the MBGs increased from 54 m^2/g to 126 (Co2.5), 76 (Cu2.5), and 194 m^2/g (Co/Cu2.5). The relevant ellipses showed that increasing S_{BET} is attributed to changing the particle morphologies. The BJH analysis demonstrated the glasses are indeed mesoporous particles (average diameter ranges from 2 nm to 50 nm). The BJH curves displayed in Fig. 2D exhibit a wide peak (B0 sample) or multi-peak profile (doped sample), suggesting that the materials are characterized by a disordered mesoporous structure. In this regard, it is worth underlining that incorporation of ions typically distorts the mesoporous structure. The composition-structure relationship was studied in silicate mesoporous glasses, which are remarkably more common than borate MBGs. It was suggested that the replacement of Ca^{2+} with other network modifiers may disrupt the ordered orientation of silicate units during the self-assembly reaction. The reason for this may be the valence difference between cations, causing defects in the atomic array and ultimately leading to alterations in the shape of the mesopore channels [44]. Similar considerations can also be applied to the borate MBGs analyzed in the present study, the compositions of which contain a large amount of modifiers (43.7 mol.%). These structural findings are also consistent with the results from thermal analysis previously discussed.

The term "bioactivity" classically refers to the apatite-forming ability (also *in vitro*) and, hence, the bone-bonding capability (*in vivo*) of bioactive materials upon exposure to biological fluids [45]. The mineralization process of bioactive materials should take place within 28 days according to ISO 23317:2014 [46]. Therefore, we evaluated the bioactivity of the SBF-immersed MBGs by using XRD and SEM analysis. As a rule of thumb, an amorphous calcium phosphate (ACP) layer forms on the surface of MBGs soaked in SBF, which then crystallizes into HAp [31]. Based on XRD data (Fig. 3), HAp is mineralized on the MBG surfaces with lattice constants of (a = 9.424-9.444, c = 6.879-6.884) (Table 3); variations in lattice constants are primarily caused by the adsorption/desorption process in SBF and released ions from the samples, which may be incorporated into the newly-mineralized HAp structures. Based on the calculations, the crystallinity of the formed HAp layer on the different glass groups increased by 60-80% after 21 days of incubation in SBF. According to Table 4 and Fig. 4, we found that the crystal growth rate of HAp varies between samples. The calculations indicated that the crystallinity rate (slope of crystallinity-time graphs) increased from 0.125 (dopant-free MBGs) to 0.155 (Co2.5), 0.137 (Cu2.5), and 0.157 (Cu/Co0.5) (Table 4). Several factors could explain these phenomena including (I) changes in the solubility of the glass caused by different chemical bonds between Co-O/Cu-O and Ca-O and (II) a reduced rate of formation of stable apatite due to dopant leaching to SBF [41,46]. It has been noted in previous studies that mineralized HAp on borate glasses has higher crystallinity than mineralized HAp on silicate glasses under similar conditions. The reason for this event is related to the incomplete conversion of silicate glasses into ACP and their slow transformation into HAp [12]. Fig. 5 illustrates the progressive mineralization of HAp onto the borate glasses and displays a globular morphology of the new phase after 21 days. SEM images suggest that the presence of dopants leads to no significant differences in terms of the morphology of the HAp formed on the various glasses, although – as revealed by XRD – an effect exists on the crystallinity. The pH measurement and its ellipse representation (Fig. 6) indicated a sharp increase in the pH values during the first 5 days (from 7.42 to 9.5), followed by some changes up to 21 days. An increase in the pH is caused by the dissolution of ions in SBF, and a decrease in the pH is due to the formation of HAp onto the glass samples. According to Figs. 7 and 8, the release profiles of the B^{3+} ions and dopants (i.e., Co^{2+} and Cu^{2+}) are highly dependent on the chemical composition of the MBGs. The incorporation of Co/Cu into BGs causes a weakness in the glass network and bond strength, thereby resulting in a higher release of the B^{3+} ions. As shown in the relevant ellipse representation, Co^{2+} ions have a greater effect on glass dissolution than Cu^{2+}; this may be due to the greater ionic radius of Co^{2+} ions compared to Cu^{2+} ions. Previous studies about melt-derived Co-doped 13-93 glasses reported that even a few ppm of Co^{2+} ions released from those materials were enough to elicit a therapeutic effect on cells [47,48]. Hence, the cobalt release profile displayed in Fig. 8 suggests the enhanced therapeutic potential of the glasses developed in the present work, confirmed by *in vitro* and *in ovo* assays. On the other hand, the release of ions, especially heavy metal ions, into biological fluids raises some concerns about the toxicity and harmful effects of the doped BGs in a medical setting (Fig. 8). However, these conditions are commonly moderated *in vivo* by high-volume fluids in the body [33]. This point is confirmed by the cytotoxicity test results (Fig. 9), in which a significant decrease in cell viability is seen after 24 h of incubation while the number of alive cells significantly increased again after 72 h. The MTT results and ellipse representation clearly illustrate how the adverse effects of burst release of ions from the MBGs are moderated over time (Fig. 9). It is crucial to investigate the biosafety of MBGs in contact with blood in light of their increasing clinical use [49,50]. The hemolysis process occurs when the membrane of the red blood cells (RBCs) breaks and hemoglobin is released into the surrounding fluids. RBC hemolysis is mentioned as an index of hemocompatibility of biomaterials [51]. As shown in Fig. 10, the hemolysis of all samples is less than 3.5%, which indicates their proper hemocompatibility. Furthermore, the attachment of cells to the surface of the synthesized MBGs was examined as another evaluation for biocompatibility. During an adhesion process, cells and material surfaces interact in a dynamic manner [52]. For this purpose, we prepared MBG pellets

and tested the adhesion of L929 cells for 72 h on their surface. Based on the test results, the cells adhered well to the MBG surfaces and expanded accordingly (Fig. 11). Different observed morphologies of cells in the samples are commonly related to different physico-chemical properties, including morphology, composition, and pore size of the MBG surfaces [53,54]. As can be observed, the morphology of the cells cultured on the doped glasses mimics their native shape *in vitro* (i.e., elongated shapes).

Infections caused by bacteria, particularly multidrug-resistant (MDR) bacteria (e.g., *S. aureus* and *P. aeruginosa*), are still a major challenge in the biomedical field, including managing surgical wounds [55]. Therefore, the prepared MBGs were tested against both Gram-positive (*S. aureus*) and Gram-negative (*P. aeruginosa*) bacteria. The results indicated that the glasses significantly reduced the viability of both bacteria, which decreased up to 11% of the control (Fig. 12). Fig. 12A and **B** presents the effect of the doped MBGs on bacteria using an ellipse representation, which relates to the different physico-chemical properties of MBGs that affect the mechanism of antibacterial activity. BGs can act against bacteria through various mechanisms, including the inhibition of cell wall and membrane synthesis, generating oxidative stress, and causing DNA damage [18]. Compared to single-doped MBGs, the Co-/Cu-doped MBGs have a greater adverse effect on the viability of bacteria, which is consistent with their higher reactivity in biological solutions; in this regard, a more marked alkaline pH (Fig. 6) is not favorable for bacteria. Furthermore, we employed disk diffusion and CFU tests to investigate the effect of MBGs on the viability of bacteria, which indicates that the MBGs are effective in inhibiting bacteria growth as well (Figs. 12C and **13**).

One of the main goals of tissue engineering strategies is to restore the structural and functional integrity of damaged tissues; this can be supported by establishing new blood vessels that can provide oxygen and nutrients to newly-formed tissues [56,57]. BGs can induce neovascularization thanks to the release of pro-angiogenic ions (e.g., B^{3+}) into the surrounding biological environment. In this study, *in vitro* scratch, and *in ovo* CAM assays were employed to assess the angiogenic potential of the synthesized borate glasses. Compared to the negative control, all MBGs could significantly stimulate the migration of HUVECs in the scratch assay (Fig. 14). The HUVEC migration increased significantly in the MBGs doped with Co^{2+} and Co^{2+}/Cu^{2+} ions compared to the dopant-free MBGs. This result was predictable since Co and Cu are known as elements with the ability to improve the angiogenesis process (e.g., overexpression and stabilization of nuclear HIF-1α and subsequently enhanced hypoxia) [18]. These results also confirm the expectations from ion release studies (Fig. 8). According to Fig. 15, the doped samples have a significant ability to induce angiogenesis *in ovo*. The CAM treated with Co-/Cu-doped MBGs exhibited the highest vascular density (131% of control). The Co-doped group also showed higher vascular density (123%) than its Cu-doped counterparts (114% of the control). In accordance with the literature, Co^{2+} ions significantly affect angiogenesis [58]. Furthermore, different shapes and diameters of the newly formed vessels may be related to the different chemical compositions of the synthesized glasses [59,60]. Lastly, all synthesized MBGs were classified based on their characteristics and cellular responses (Fig. 16). A K-means clustering algorithm showed that dopant-free MBGs are in an independent group, suggesting that the dopants have a high impact on the MBG properties. Similarly, Co/Cu2.5 clustered into an independent group based on this clustering. The overall results of these MBGs, and especially the promising biological results, motivate the need for future *in vivo* studies on such materials.

5. Conclusions

In this study, Co- and Cu-doped 13-93B3 MBGs were synthesized and examined using computational and biological approaches. Based on the physico-chemical analyses, the synthesized MBGs have T_g values within 539-773 °C, surface charges ranging from -12 to -43 mV, S_{BET} values ranging from 54 to 194 m^2/g, and pore diameters ranging from 5 to 23 nm. The significant improvement in physico-chemical properties is attributed to the fact that the dopants have a significant impact on oxygen packing density, bond length, non-bridging oxygen concentrations (NBOs), ion mobility, configurational entropy (S_{Conf}), boron-boron separation, and repulsion force in the glass network. Upon immersion of the doped MBGs in biological solutions, a sharp increase in the pH values occurred after five days which was associated with a burst release of ions. Based on the results of the *in vitro* biocompatibility tests, the prepared glasses had no significant adverse effects on the fibroblast and red blood cells. Importantly, the prepared borate MBGs exhibited high antibacterial effects against both Gram-positive (*S. aureus*) and Gram-negative bacteria (*P. aeruginosa*). Moreover, we found that the glass samples can improve angiogenesis as they enhanced the migration of HUVECs *in vitro* and increased vascular density within CAM *in ovo*. It was noted that the MBGs co-doped with Cu and Co elicit higher antibacterial and pro-angiogenic effects compared to the other materials due to the synergistic actions of dopants. *In vivo* experiments may help determine the actual potential of this type of glasses for managing hard and/or soft tissue injuries.

Declaration of competing interest

The authors declare that they have no known competing financial interests or personal relationships that could have appeared to influence the work reported in this paper.

Acknowledgments

This study was kindly supported by the Mashhad University of Medical Sciences through research grant number 400453.

References

[1] J. Bonnell, M. Ogihara, Y. Yesha, Challenges and issues in data science education, Computer 55 (2022) 63–66, https://doi.org/10.1109/mc.2021.3128734.
[2] F. Qin, J. Li, C. Zhang, G. Zeng, D. Huang, X. Tan, D. Qin, H. Tan, Biochar in the 21st century: a data-driven visualization of collaboration, frontier identification, and future trend, Sci. Total Environ. 818 (2022), 151774, https://doi.org/10.1016/j.scitotenv.2021.151774.
[3] S.V.G. Subrahmanya, D.K. Shetty, V. Patil, B.M.Z. Hameed, R. Paul, K. Smriti, N. Naik, B.K. Somani, The role of data science in healthcare advancements: applications, benefits, and future prospects, Ir. J. Med. Sci. 191 (2022) 1473–1483, https://doi.org/10.1007/s11845-021-02730-z.
[4] S. Maheshwari, P. Gautam, C.K. Jaggi, Role of Big Data Analytics in supply chain management: current trends and future perspectives, Int. J. Prod. Res. 59 (2020) 1875–1900, https://doi.org/10.1080/00207543.2020.1793011.
[5] S. Sajid, A. Haleem, S. Bahl, M. Javaid, T. Goyal, M. Mittal, Data science applications for predictive maintenance and materials science in context to Industry 4.0, Mater. Today: Proc. 45 (2021) 4898–4905, https://doi.org/10.1016/j.matpr.2021.01.357.
[6] B. Basu, N.H. Gowtham, Y. Xiao, S.R. Kalidindi, K.W. Leong, Biomaterialomics: data science-driven pathways to develop fourth-generation biomaterials, Acta Biomater. 143 (2022) 1–25, https://doi.org/10.1016/j.actbio.2022.02.027.
[7] D. Minh, H.X. Wang, Y.F. Li, T.N. Nguyen, Explainable artificial intelligence: a comprehensive review, Artif. Intell. Rev. 55 (2021) 3503–3568, https://doi.org/10.1007/s10462-021-10088-y.
[8] Z. Mollaei, F. Kermani, F. Moosavi, M. Kahani, S. Mollazadeh, J. Vahdati Khaki, Elaboration of entropy with glass composition: a molecular dynamics study, Mater. Today Commun. 33 (2022), https://doi.org/10.1016/j.mtcomm.2022.104340.
[9] Z. Mollaei, F. Kermani, M. Kahani, F. Moosavi, S. Mollazadeh, J. Vahdati Khaki, Configurational entropy as a simple input data for glass science and engineering, Mater. Today Commun. 32 (2022), https://doi.org/10.1016/j.mtcomm.2022.104153.
[10] A. Fathi, F. Kermani, A. Behnamghader, S. Banijamali, M. Mozafari, F. Baino, S. Kargozar, Three-dimensionally printed polycaprolactone/multicomponent bioactive glass scaffolds for potential application in bone tissue engineering, Biomedical Glasses 6 (2020) 57–69, https://doi.org/10.1515/bglass-2020-0006.
[11] F. Baino, S. Kargozar, Bioactive Glasses and Glass-Ceramics: Fundamentals and Applications, John Wiley & Sons, 2022.
[12] D. Ege, K. Zheng, A.R. Boccaccini, Borate bioactive glasses (BBG): bone regeneration, wound healing applications, and future directions, ACS Appl. Bio Mater. 5 (2022) 3608–3622, https://doi.org/10.1021/acsabm.2c00384.
[13] F. Kermani, H. Sadidi, A. Ahmadabadi, S.J. Hoseini, S.H. Tavousi, A. Rezapanah, S. Nazarnezhad, S.A. Hosseini, S. Mollazadeh, S. Kargozar, Modified sol–gel synthesis of mesoporous borate bioactive glasses for potential use in wound

healing, Bioengineering 9 (2022), https://doi.org/10.3390/bioengineering9090442.
[14] S. Yamaguchi, Borate Bioactive Glass, Bioactive Glasses and Glass-Ceramics, 2022, pp. 79–86.
[15] W.C. Lepry, S.N. Nazhat, A review of phosphate and borate sol–gel glasses for biomedical applications, Advanced NanoBiomed Research 1 (2021), https://doi.org/10.1002/anbr.202000055.
[16] M. Bengisu, Borate glasses for scientific and industrial applications: a review, J. Mater. Sci. 51 (2015) 2199–2242, https://doi.org/10.1007/s10853-015-9537-4.
[17] W.C. Lepry, S.N. Nazhat, Highly bioactive sol-gel-derived borate glasses, Chem. Mater. 27 (2015) 4821–4831, https://doi.org/10.1021/acs.chemmater.5b01697.
[18] S. Kargozar, M. Montazerian, S. Hamzehlou, H.W. Kim, F. Baino, Mesoporous bioactive glasses: promising platforms for antibacterial strategies, Acta Biomater. 81 (2018) 1–19, https://doi.org/10.1016/j.actbio.2018.09.052.
[19] E.D. Zanotto, F.A.B. Coutinho, How many non-crystalline solids can be made from all the elements of the periodic table? J. Non-Cryst. Solids 347 (2004) 285–288, https://doi.org/10.1016/j.jnoncrysol.2004.07.081.
[20] E. Alcobaça, S.M. Mastelini, T. Botari, B.A. Pimentel, D.R. Cassar, A.C.P.d.L.F. de Carvalho, E.D. Zanotto, Explainable machine learning algorithms for predicting glass transition temperatures, Acta Mater. 188 (2020) 92–100, https://doi.org/10.1016/j.actamat.2020.01.047.
[21] M.B. Taye, Biomedical applications of ion-doped bioactive glass: a review, Appl. Nanosci. 12 (2022) 3797–3812, https://doi.org/10.1007/s13204-022-02672-7.
[22] F. Kermani, S. Nazarnezhad, Z. Mollaei, S. Mollazadeh, A. Ebrahimzadeh-Bideskan, V.R. Askari, R.K. Oskuee, A. Moradi, S.A. Hosseini, Z. Azari, F. Baino, S. Kargozar, Zinc- and copper-doped mesoporous borate bioactive glasses: promising additives for potential use in skin wound healing applications, Int. J. Mol. Sci. 24 (2023), https://doi.org/10.3390/ijms24021304.
[23] F. Kermani, S. Mollazadeh Beidokhti, F. Baino, Z. Gholamzadeh-Virany, M. Mozafari, S. Kargozar, Strontium- and cobalt-doped multicomponent mesoporous bioactive glasses (MBGs) for potential use in bone tissue engineering applications, Materials 13 (2020), https://doi.org/10.3390/ma13061348.
[24] S. Kargozar, N. Lotfibakhshaiesh, J. Ai, M. Mozafari, P. Brouki Milan, S. Hamzehlou, M. Barati, F. Baino, R.G. Hill, M.T. Joghataei, Strontium- and cobalt-substituted bioactive glasses seeded with human umbilical cord perivascular cells to promote bone regeneration via enhanced osteogenic and angiogenic activities, Acta Biomater. 58 (2017) 502–514, https://doi.org/10.1016/j.actbio.2017.06.021.
[25] S. Kargozar, M. Mozafari, S. Ghodrat, E. Fiume, F. Baino, Copper-containing bioactive glasses and glass-ceramics: from tissue regeneration to cancer therapeutic strategies, Mater. Sci. Eng. C (2021) 121, https://doi.org/10.1016/j.msec.2020.111741.
[26] Y.-C. Huang, T.-Y. Lin, S.-C. Huang, T.-Y. Yang, C.-J. Shih, Copper-enhanced silver releasing from bimetal-containing bioactive glass (AgCu/80S) elicits antibacterial efficacy against drug-resistant Staphylococcus aureus, J. Non-Cryst. Solids 584 (2022), https://doi.org/10.1016/j.jnoncrysol.2022.121509.
[27] M.L. Ermini, V. Voliani, Antimicrobial nano-agents: the copper age, ACS Nano 15 (2021) 6008–6029, https://doi.org/10.1021/acsnano.0c10756.
[28] M. Dziadek, B. Zagrajczuk, E. Menaszek, K. Dziadek, K. Cholewa-Kowalska, A simple way of modulating in vitro angiogenic response using Cu and Co-doped bioactive glasses, Mater. Lett. 215 (2018) 87–90, https://doi.org/10.1016/j.matlet.2017.12.075.
[29] S. Jana, P. Datta, H. Das, P.R. Ghosh, B. Kundu, S.K. Nandi, Engineering vascularizing electrospun dermal grafts by integrating fish collagen and ion-doped bioactive glass, ACS Biomater. Sci. Eng. 8 (2022) 734–752, https://doi.org/10.1021/acsbiomaterials.1c01098.
[30] T. Kokubo, H. Takadama, How useful is SBF in predicting in vivo bone bioactivity? Biomaterials 27 (2006) 2907–2915, https://doi.org/10.1016/j.biomaterials.2006.01.017.
[31] M. Mozafari, S. Banijamali, F. Baino, S. Kargozar, R.G. Hill, Calcium carbonate: adored and ignored in bioactivity assessment, Acta Biomater. 91 (2019) 35–47, https://doi.org/10.1016/j.actbio.2019.04.039.
[32] S. Nazarnezhad, F. Kermani, V.R. Askari, S.A. Hosseini, A. Ebrahimzadeh-Bideskan, A. Moradi, R. Kazemi Oskuee, S. Mollazadeh, S. Kargozar, Preparation and characterization of platelet lysate (Pl)-Loaded electrospun nanofibers for epidermal wound healing, J. Pharmaceut. Sci. 111 (2022) 2531–2539, https://doi.org/10.1016/j.xphs.2022.04.008.
[33] F. Hohenbild, M. Arango-Ospina, A. Moghaddam, A.R. Boccaccini, F. Westhauser, Preconditioning of bioactive glasses before introduction to static cell culture: what is really necessary? Methods Protoc 3 (2020) https://doi.org/10.3390/mps3020038.
[34] S.A. Hosseini, S. Javad Hoseini, V.R. Askari, R. Salarinia, A. Ebrahimzadeh-Bideskan, F. Tara, F. Kermani, S. Nazarnezhad, S. Kargozar, Pectin-reinforced electrospun nanofibers: fabrication and characterization of highly biocompatible mats for wound healing applications, J. Drug Deliv. Sci. Technol. 77 (2022), https://doi.org/10.1016/j.jddst.2022.103916.
[35] A. Jacobs, G. Renaudin, C. Forestier, J.-M. Nedelec, S. Descamps, Biological properties of copper-doped biomaterials for orthopedic applications: a review of antibacterial, angiogenic and osteogenic aspects, Acta Biomater. 117 (2020) 21–39, https://doi.org/10.1016/j.actbio.2020.09.044.
[36] S. Ibrahim, F.I. El-Agawany, Y.S. Rammah, E.M. Ahmed, A.A. Ali, ZnO-Bi2O3-B2O3 glasses doped with rare earth oxides: synthesis, physical, structural characteristics, neutron and photon attenuation attitude, Optik 243 (2021), https://doi.org/10.1016/j.ijleo.2021.167414.
[37] P. Dixit Shweta, A. Singh, S.K. Avinashi, B.C. Yadav, C. Gautam, Fabrication, structural, and physical properties of alumina doped calcium silicate glasses for carbon dioxide gas sensing applications, J. Non-Cryst. Solids 583 (2022), https://doi.org/10.1016/j.jnoncrysol.2022.121475.
[38] C. Gautam, A.K. Yadav, A.K. Singh, A review on infrared spectroscopy of borate glasses with effects of different additives, ISRN Ceramics 2012 (2012) 1–17, https://doi.org/10.5402/2012/428497.
[39] R. Divina, G. Sathiyapriya, K. Marimuthu, A. Askin, M.I. Sayyed, Structural, elastic, optical and γ-ray shielding behavior of Dy3+ ions doped heavy metal incorporated borate glasses, J. Non-Cryst. Solids 545 (2020), https://doi.org/10.1016/j.jnoncrysol.2020.120269.
[40] A. Pedone, The antioxidant properties of Ce-containing bioactive glass nanoparticles explained by Molecular Dynamics simulations, Biomedical glasses 2 (2016), https://doi.org/10.1515/bglass-2016-0003/html.
[41] F. Kermani, A. Vojdani-Saghir, S. Mollazadeh Beidokhti, S. Nazarnezhad, Z. Mollaei, S. Hamzehlou, A. El-Fiqi, F. Baino, S. Kargozar, Iron (Fe)-doped mesoporous 45S5 bioactive glasses: implications for cancer therapy, Transl Oncol 20 (2022), 101397, https://doi.org/10.1016/j.tranon.2022.101397.
[42] E.M. Moreno, M. Zayat, M.P. Morales, C.J. Serna, A. Roig, D. Levy, Preparation of narrow size distribution superparamagnetic γ-Fe2O3 nanoparticles in a Sol−Gel transparent SiO2 matrix, Langmuir 18 (2002) 4972–4978, https://doi.org/10.1021/la020037s.
[43] S. Metwally, U. Stachewicz, Surface potential and charges impact on cell responses on biomaterials interfaces for medical applications, Mater. Sci. Eng., C 104 (2019), 109883, https://doi.org/10.1016/j.msec.2019.109883.
[44] C. Wu, W. Fan, Y. Zhu, M. Gelinsky, J. Chang, G. Cuniberti, V. Albrecht, T. Friis, Y. Xiao, Multifunctional magnetic mesoporous bioactive glass scaffolds with a hierarchical pore structure, Acta Biomater. 7 (2011) 3563–3572, https://doi.org/10.1016/j.actbio.2011.06.028.
[45] M.P. Ginebra, E.B. Montufar, Injectable Biomedical Foams for Bone Regeneration, Biomedical Foams for Tissue Engineering Applications, 2014, pp. 281–312.
[46] S. Kargozar, P.B. Milan, M. Amoupour, F. Kermani, S. Gorgani, S. Nazarnezhad, S. Hooshmand, F. Baino, Osteogenic potential of magnesium (Mg)-Doped multicomponent bioactive glass: in vitro and in vivo animal studies, Materials 15 (2022), https://doi.org/10.3390/ma15010318.
[47] A. Hoppe, B. Jokic, D. Janackovic, T. Fey, P. Greil, S. Romeis, J. Schmidt, W. Peukert, J. Lao, E. Jallot, A.R. Boccaccini, Cobalt-Releasing 1393 bioactive glass-derived scaffolds for bone tissue engineering applications, ACS Appl. Mater. Interfaces 6 (2014) 2865–2877, https://doi.org/10.1021/am405354y.
[48] A. Hoppe, A. Brandl, O. Bleiziffer, A. Arkudas, R.E. Horch, B. Jokic, D. Janackovic, A.R. Boccaccini, In vitro cell response to Co-containing 1393 bioactive glass, Mater. Sci. Eng. C 57 (2015) 157–163, https://doi.org/10.1016/j.msec.2015.07.014.
[49] S.K. Arepalli, H. Tripathi, S.K. Hira, P.P. Manna, R. Pyare, S.P. Singh, Enhanced bioactivity, biocompatibility and mechanical behavior of strontium substituted bioactive glasses, Mater. Sci. Eng., C 69 (2016) 108–116, https://doi.org/10.1016/j.msec.2016.06.070.
[50] S. Majumdar, S.K. Hira, H. Tripathi, A.S. Kumar, P.P. Manna, S.P. Singh, S. Krishnamurthy, Synthesis and characterization of barium-doped bioactive glass with potential anti-inflammatory activity, Ceram. Int. 47 (2021) 7143–7158, https://doi.org/10.1016/j.ceramint.2020.11.068.
[51] M.A. Dobrovolskaia, J.D. Clogston, B.W. Neun, J.B. Hall, A.K. Patri, S.E. McNeil, Method for analysis of nanoparticle hemolytic properties in vitro, Nano Lett. 8 (2008) 2180–2187, https://doi.org/10.1021/nl0805615.
[52] M. Lotfi, M. Nejib, M. Naceur, Cell adhesion to biomaterials: concept of biocompatibility, in: R. Pignatello, Editor. InTech, Rijeka (Croatia) (Eds.), Advances in Biomaterials Science and Biomedical Applications, 2013, pp. 207–240.
[53] U. Thamma, T.J. Kowal, M.M. Falk, H. Jain, Nanostructure of bioactive glass affects bone cell attachment via protein restructuring upon adsorption, Sci. Rep. 11 (2021) 5763, https://doi.org/10.1038/s41598-021-85050-7.
[54] J.E. Gough, I. Notingher, L.L. Hench, Osteoblast attachment and mineralized nodule formation on rough and smooth 45S5 bioactive glass monoliths, J. Biomed. Mater. Res. 68 (2004) 640–650, https://doi.org/10.1002/jbm.a.20075.
[55] C.K. Sen, Human wound and its burden: updated 2020 compendium of estimates, Adv. Wound Care 10 (2021) 281–292, https://doi.org/10.1089/wound.2021.0026.
[56] S. Kargozar, F. Baino, S. Hamzehlou, M.R. Hamblin, M. Mozafari, Nanotechnology for angiogenesis: opportunities and challenges, Chem. Soc. Rev. 49 (2020) 5008–5057, https://doi.org/10.1039/c8cs01021h.
[57] F. Kermani, S. Mollazadeh, S. Kargozar, J. Vahdati Khakhi, Improved osteogenesis and angiogenesis of theranostic ions doped calcium phosphates (CaPs) by a simple surface treatment process: a state-of-the-art study, Mater. Sci. Eng. C (2021) 124, https://doi.org/10.1016/j.msec.2021.112082.
[58] H. Zhang, Y. Zhao, Y. Zhang, R. Hang, X. Yao, R. Hang, Exosomes derived from macrophages upon cobalt ion stimulation promote angiogenesis, Colloids Surf. B Biointerfaces 203 (2021), 111742, https://doi.org/10.1016/j.colsurfb.2021.111742.
[59] G.E. Vargas, L.A. Haro Durand, V. Cadena, M. Romero, R.V. Mesones, M. Mackovic, S. Spallek, E. Spiecker, A.R. Boccaccini, A.A. Gorustovich, Effect of nano-sized bioactive glass particles on the angiogenic properties of collagen based composites, J. Mater. Sci. Mater. Med. 24 (2013) 1261–1269, https://doi.org/10.1007/s10856-013-4892-7.
[60] D. Dhinasekaran, S. Vimalraj, A.R. Rajendran, S. Saravanan, B. Purushothaman, B. Subramaniam, Bio-inspired multifunctional collagen/electrospun bioactive glass membranes for bone tissue engineering applications, Mater. Sci. Eng., C 126 (2021), 111856, https://doi.org/10.1016/j.msec.2020.111856.